CHAPTER 11

The Seismic Source: Dynamics

Seismic waves propagate in ways that are largely governed by the relationship $\rho\ddot{u}_i = \tau_{ji,j}$ between acceleration and stress gradient, and by the relationship between stress and strain known as Hooke's law (2.18). But in the source region of a particular earthquake, Hooke's law fails. If we are to reach a quantitative understanding of the ground motions that result from that earthquake, we need to replace Hooke's law by some other relationship that accurately determines stress as a function of the deformation of materials within the source region—or, that determines deformation as a function of stress.

So far we have suppressed the difficulties of this problem, because to interpret the seismograms from one particular earthquake in detail, within the framework of Green functions weighted by a displacement discontinuity across a fault surface, we saw in Section 2.5 and Chapter 3 that we all we need to know is the fault slip as a function of space and time on the fault. See equation (3.2), with which we started Chapter 10 on source kinematics, allowing us to study the seismic motion at near and far field for a propagating dislocation in cases where the slip function has already been specified—or at least parameterized in a particular way. The form of the slip function was adopted intuitively to simulate geologic faulting with the least number of parameters, preferably ones that could be determined from analysis of the resulting seismic radiation. But unfortunately, some of the slip functions analyzed in Chapter 10 turn out to have consequences that are physically unacceptable.

Take the simplest case of an anti-plane problem in which a semi-infinite fault is propagating with uniform velocity (Section 10.2.3). When the slip occurs as a step function, the shear stress acting on the fault plane is given by equation (10.46),

$$\tau_{yz} = \mu \frac{\Delta w}{2\pi} \frac{\sqrt{1 - v^2/\beta^2}}{x'} \qquad \text{(putting } x' = x - vt\text{)}. \tag{11.1}$$

We expect that the fault plane, once ruptured, cannot sustain stress greater than the frictional stress. But according to (11.1), the shear stress has nonzero values inside the fault plane ($x' < 0$), becoming larger and larger without limit on the fault plane as the crack tip is approached (i.e., as $x' \to 0$ from below). Obviously, then, the assumption of step-function slip leads to a gross violation of physical expectation. In this chapter we shall develop a

variety of better alternatives to step-function slip, with the principal aim of finding fault motions that not only are kinematically satisfactory for shear failure, but are also associated with plausible stresses on the fault plane.

In considering the failure of Hooke's law for a particular earthquake, we can regard the fault plane—which will eventually rupture—as a surface of weakness. For example, as stress slowly rises in the source region due to tectonic processes, we may assume that the capacity of frictional stress to resist the growing shearing stress is eventually exceeded. It is the pre-existing fault surface that fails rather than another surface, precisely because the fault is relatively weak. But how does the failure actually take place? As stress rises during the tectonic loading process over a period of perhaps decades, does strain generally stay proportional to stress, or is there a tendency for some ductility (in which strain rate would be nonzero at fixed high stress, even if the stress were constant)? Even if there is no ductility, does strain stay proportional to stress right up to the instant of failure, or do materials in the source region exhibit a nucleation process in which strain departs slightly from the linearity predicted by Hooke's law, just prior to failure? If there is a nucleation process, then what is its time scale and its dependence on stress relative to a critical stress? If failure occurs and stress levels on the fault surface drop from their static frictional values as fault slip begins, then how quickly do they drop, what is the value of frictional resistance during the actual process of fault slip, and how do stress levels continue to change as fault slip comes to a halt?

These questions on material properties have long been the subject of laboratory experiment. Many observations are summarized by Coulomb's law of friction, stating that frictional resistance to one object sliding over another is proportional to the net force bringing the two objects into contact. The expression of Coulomb's law in seismology is that the frictional shearing stress between the two faces of a fault surface is proportional to the normal stress. As reviewed by Scholz (1998), in the standard model of stick-slip friction it is assumed that sliding begins when the ratio of shear stress to normal stress reaches a value μ_s, called the static friction coefficient. Once sliding begins, frictional resistance falls to a lower value so that the coefficient of dynamic friction, μ_d, is less than μ_s. An instability can result, leading to slip propagation and all the phenomena of fault rupture and associated radiation of seismic waves.

It has been found experimentally that μ_s is greater the longer the fault surfaces have been in contact without sliding. Furthermore, the value of μ_d depends on the relative velocity with which the fault surface slides. The general subject of fault constitutive laws has been developed extensively by Dieterich and others (see Dieterich, 1981; Ruina, 1983; Sleep, 1987, Marone, 1998; and Dieterich and Kilgore, 1996). As we shall see in considering particular examples, there is often a question as to whether the details of some particular relationship between fault slip and fault stress can be inferred from properties of the resulting seismic waves, or whether these details entail time scales and length scales too short to measure from the radiated signals. In the latter case, progress will more likely come from extrapolation of phenomena measured in the laboratory—over scales on the order of a meter or much less—up to scales on the order of a kilometer or much more, as needed in application to earthquakes of significant size.

This chapter studies simple models of dynamic faulting in two main sections, followed by a shorter section that outline features of more complicated models. Thus in Section 11.1 we shall suppose that the rupture velocity has been prescribed (usually, we shall assume

it has some constant value). We obtain a simple relation between slip and shear stress on a fault plane for anti-plane problems. Then we describe the energy balance at the rupture front for anti-plane and in-plane faulting, and introduce the concept of cohesive force. As a useful illustration of rupture propagation that originates from a point (and therefore involves both anti-plane and in-plane motions), we look at the case of a growing elliptical fault, for which the radiated motions are known in detail. As an example of a fault that grows steadily (from a point) and then suddenly stops, we describe a growing circular fault with known final radius and use an important numerical procedure to obtain the far-field motions. In the second main section, we recognize that shear failure is a spontaneous process and that the velocity of rupture is itself an unknown and probably varying quantity, to be determined as part of the solution to the problem in hand. The rupture-velocity history is known for a variety of anti-plane problems and for certain in-plane problems. Our intent in these Sections 11.1 and 11.2 is to develop analytical methods that provide ways to explore a variety of relationships between fault stress and fault slip or slip velocity.

In consideration of the dynamics of a particular earthquake, it is vastly simplifying to restrict attention to situations in which normal stress is unchanged by the faulting process. But as we point out in Section 11.3, there are a number of important situations in which normal stress is itself changed by faulting.

11.1 Dynamics of a Crack Propagating with Prescribed Velocity

11.1.1 RELATIONS BETWEEN STRESS AND SLIP FOR A PROPAGATING CRACK

In order to find an appropriate slip function for a crack propagating with a constant velocity v, we shall first find a relationship between the stress and slip on the fault plane for a propagating anti-plane dislocation.

Let the slip function $\Delta w(x')$ be an arbitrary function. We shall express $\Delta w(x')$ by a superposition of step functions, as shown in Figure 11.1. An arbitrary $\Delta w(x')$ can be written as

$$\Delta w(x') = -\int_{x'}^{0} \frac{\partial\, \Delta w}{\partial \xi}\, d\xi = -\int_{-\infty}^{0} \frac{\partial\, \Delta w}{\partial \xi} H(\xi - x')\, d\xi. \tag{11.2}$$

The step-function slip $H(\xi - x')$ with tip at $x' = \xi$ will generate a stress component τ_{yz} according to equation (11.1) given by

$$\tau_{yz}(x', \xi) = \frac{\mu}{2\pi} \cdot \frac{\sqrt{1 - v^2/\beta^2}}{x' - \xi}.$$

Multiplying by the step height $-(\partial\, \Delta w/\partial \xi)\, d\xi$ and integrating over ξ from $-\infty$ to 0, we find that the stress due to the slip function $\Delta w(x')$ is

$$\tau_{yz}(x') = -\frac{\mu}{2\pi}\sqrt{1 - v^2/\beta^2} \int_{-\infty}^{0} \frac{\partial\, \Delta w/\partial \xi}{x' - \xi}\, d\xi = -\frac{\mu}{2\pi} \frac{\sqrt{1 - v^2/\beta^2}}{v} \int_{-\infty}^{0} \frac{\Delta \dot{w}}{\xi - x'}\, d\xi, \tag{11.3}$$

where $\Delta \dot{w}$ is the slip velocity.

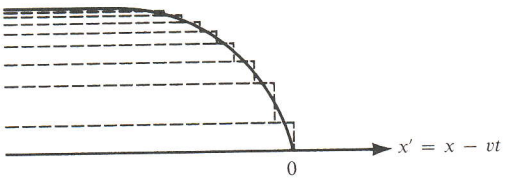

FIGURE **11.1**
Approximating an arbitrary slip function $\Delta w(x')$ by a superposition of step functions.

For the in-plane problem, a similar relation is found between the shear stress τ_{xy} on the fault plane and slip velocity $\Delta\dot{w}$. Applying the same superposition to equation (10.65), we get

$$\tau_{xy}(x') = -\frac{2\mu\beta^2}{\pi v^3}\left[\sqrt{1-v^2/\alpha^2} - \frac{(1-v^2/2\beta^2)^2}{\sqrt{1-v^2/\beta^2}}\right]\int_{-\infty}^{0}\frac{\Delta\dot{u}}{\xi - x'}d\xi. \qquad (11.4)$$

In both (11.3) and (11.4), we see that the shear stress on the fault plane is a constant times the Hilbert transform of slip velocity.

A function and its Hilbert transform are very closely related. From Box 5.6, we see that if $g(x)$ is the Hilbert transform of a function $f(x)$, then these two function share a common amplitude spectral density, and their spectral phases differ by $\pi/2$.

Thus the shear stress and the slip velocity on the plane $y = 0$ must share a common amplitude spectral density apart from a constant factor, with a phase difference of $\pi/2$. Furthermore, the slip velocity must be zero outside the crack (because no slip occurs there yet), and the shear stress must be zero inside the crack (assuming no frictional stress for simplicity). In other words, we want to find a pair of functions $f(x)$ and $g(x)$ that satisfy

$$f(x) = 0 \text{ if } x > 0, \qquad g(x) = 0 \text{ if } < 0, \qquad \text{and} \qquad g(x) = \frac{1}{\pi}\int_{-\infty}^{\infty}\frac{f(\xi)}{\xi - x}d\xi. \qquad (11.5)$$

From tables of Hilbert transforms, we find that the following choices of $f(x)$ and $g(x)$ satisfy these three conditions:

$$f(x) = \frac{H(-x)}{\sqrt{-x}} \qquad \text{and} \qquad g(x) = \frac{-H(x)}{\sqrt{x}}.$$

It is easy to show that they satisfy the integral in equation (11.5) by extending ξ to a complex plane and making a branch cut along the negative real axis (Fig. 11.2). The integral along AO will be equal to the one along OB because of the opposite signs of $\sqrt{-\xi}$ on the two paths. For $x > 0$, the residue evaluation of $\xi = x$ gives $g(x) = 1/\sqrt{x}$, and for $x < 0$ the integral vanishes because the pole is outside the contour.

Thus we find for our mechanics problem that the boundary conditions for a moving crack are satisfied by a square-root singularity in stress ahead of the crack tip, and another square-root singularity in slip velocity behind the crack tip. The square-root singularity in stress is well known for a static crack.

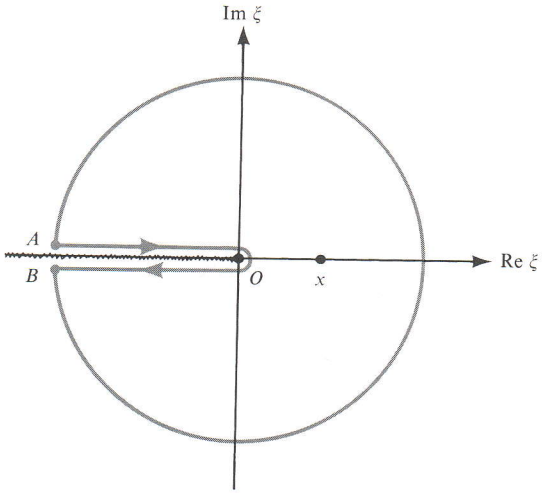

FIGURE **11.2**
Integration path for (11.5) when $f(\xi) = H(-\xi)\sqrt{-\xi}$.

By integrating the slip velocity, we find that the slip itself is proportional to $\sqrt{-x'}$ for $x' < 0$. We can now summarize results for the anti-plane case as

$$\Delta w = A\sqrt{-x'}H(-x'), \qquad \Delta \dot{w} = \frac{Av}{2\sqrt{-x'}}H(-x'), \qquad \text{and} \qquad \tau_{yz} = \frac{K}{\sqrt{2\pi x'}}H(x'),$$

where (11.6)

$$K = \sqrt{2\pi}\,\frac{\mu A\sqrt{1 - v^2/\beta^2}}{4},$$

and the in-plane case as

$$\Delta u = A'\sqrt{-x'}H(-x'), \qquad \Delta \dot{u} = \frac{A'v}{2\sqrt{-x'}}H(-x'), \qquad \text{and} \qquad \tau_{xy} = \frac{K'}{\sqrt{2\pi x'}}H(x'),$$

where (11.7)

$$K' = \sqrt{2\pi}\,\frac{\mu A'\beta^2\left[\sqrt{1 - v^2/\alpha^2} - (1 - v^2/2\beta^2)^2/\sqrt{1 - v^2/\beta^2}\right]}{v^2}.$$

The coefficients K and K' are called *stress-intensity factors* in fracture mechanics.

Note that K is zero for $v = \beta$. And since

$$K' = -\tfrac{1}{4}\sqrt{2\pi}\mu A'\beta^2 v^2 \mathsf{R}(1/v)/\sqrt{1 - v^2\beta^2},$$

where R is the Rayleigh function introduced in (5.56), we find that the stress singularity ahead of the in-plane crack is zero for rupture speed $v = c_{\mathrm{R}}$, the Rayleigh wave speed.

In the preceding chapter, we studied seismic motion from a propagating dislocation with step-function slip. Now that we have found a more appropriate slip function for the

BOX **11.1**

Stress singularities for static, in-plane, and anti-plane shear cracks of finite width 2a.

The equilibrium equation for the anti-plane displacement $w(x, y)$ is given by

$$\frac{\partial^2 w}{\partial x^2} + \frac{\partial^2 w}{\partial y^2} = 0. \tag{1}$$

For a crack plane defined by $|x| < a$, $y = 0$, and a uniform stress τ_∞ acting at $x \to \infty$ and $y \to \infty$, the boundary conditions for a stress-free crack are

$$\frac{\partial w}{\partial y} = 0 \qquad |x| < a, y = 0, \tag{2}$$

and

$$w \to \frac{\tau_\infty}{\mu} y \qquad \text{as } x, y \to \infty. \tag{3}$$

(The reference state for displacement is here taken as the stress-free state, in contrast with many of the dynamic solutions in this chapter and the previous one, where the reference state is the static strained state just prior to crack growth.)

Equation (1) can be satisfied by the real or imaginary part of an analytic function of $z = x + iy$. It is easy to show that the imaginary part of

$$f(x + iy) = \frac{\tau_\infty}{\mu}\sqrt{(x + iy)^2 - a^2} \tag{4}$$

satisfies equations (1), (2), and (3). So

$$\begin{aligned} w &= \text{Im } f(x + iy) \\ &= \frac{\tau_\infty}{\mu}\text{Im}\{[(x^2 - y^2 - a^2)^2 + 4x^2y^2]^{1/4} e^{i\theta/2}\}, \end{aligned} \tag{5}$$

where $\sin\theta = 2xy \Big/ \sqrt{(x^2 - y^2 - a^2)^2 + 4x^2y^2}$. We then have

$$\begin{aligned} w &= \frac{\tau_\infty}{\mu}\sqrt{a^2 - x^2} \qquad y = +0, |x| < a \\ &= -\frac{\tau_\infty}{\mu}\sqrt{a^2 - x^2} \qquad y = -0, |x| < a. \end{aligned} \tag{6}$$

The stress on the plane $y = 0$, but outside of the crack, is

$$\mu \frac{\partial w}{\partial y}\bigg|_{y=0} = \tau_\infty \frac{x}{\sqrt{x^2 - a^2}} \qquad |x| > a. \tag{7}$$

Here we find the square-root singularity of stress at both ends of the crack $x = a$. The stress intensity factor is $\tau_\infty\sqrt{\pi a}$, and grows in proportion to the square root of the crack

(continued)

BOX **11.1** *(continued)*

length a. The above solution was given by Knopoff (1958). A solution for an in-plane shear crack was given by Starr (1928), with the following results:

$$\begin{aligned} u &= \frac{\tau_\infty}{2}\frac{\lambda+2\mu}{\mu(\lambda+\mu)}\sqrt{a^2-x^2} \qquad y=+0,\ |x|<a \\ &= -\frac{\tau_\infty}{2}\frac{\lambda+2\mu}{\mu(\lambda+\mu)}\sqrt{a^2-x^2} \qquad y=-0,\ |x|<a \end{aligned} \tag{8}$$

and

$$\tau_{xy} = \tau_\infty \frac{x}{\sqrt{x^2-a^2}} \qquad y=0,\ |x|>a. \tag{9}$$

crack in the form $\sqrt{-x'}\,H(-x')$ (instead of $H(-x')$), we shall re-examine the motion in the vicinity of the fault. Using equation (11.2), we can express the slip function for the moving crack as a superposition of step functions:

$$A\sqrt{-x'}H(-x') = \frac{A}{2}\int_{-\infty}^{0}\frac{1}{\sqrt{-\xi}}H(\xi-x')\,d\xi.$$

Since our system is linear, if the seismic motion corresponding to unit step-function slip $H(-x')$ was $f(x', y)$, then the motion $g(x', y)$ for the moving crack will be

$$g(x', y) = \frac{A}{2}\int_{-\infty}^{0}\frac{1}{\sqrt{-\xi}}f(x'-\xi, y)\,d\xi. \tag{11.8}$$

Using this relation, we can obtain the motion and stress around the tip of the anti-plane crack from the results previously obtained for a step-function dislocation. Putting equations (10.47) and (10.45) into $f(x', y)$ of equation (11.8), the particle velocity $\dot{w}$ and stress component τ_{yz} for the moving crack can be written as

$$\dot{w} = \frac{Av}{4\pi}\int_{-\infty}^{0}\frac{1}{\sqrt{-\xi}}\frac{\gamma y\,d\xi}{(x'-\xi)^2+\gamma^2y^2} \quad \text{and} \quad \tau_{yz} = \frac{A\mu}{4\pi}\int_{-\infty}^{0}\frac{1}{\sqrt{-\xi}}\frac{\gamma(x'-\xi)\,d\xi}{(x'-\xi)^2+\gamma^2y^2}$$

where $\gamma = \sqrt{1-v^2/\beta^2}$. Both integrals can be evaluated easily by using the contour shown in Figure 11.2. Now poles are located at $\xi = x' \pm i\gamma y$, and the evaluation of residues at these poles gives

$$\dot{w} = \frac{Av}{4}\left(\frac{1}{2i\sqrt{x'-i\gamma y}} - \frac{1}{2i\sqrt{x'+i\gamma y}}\right) = \frac{Av}{4\sqrt{2}}\frac{\sqrt{\sqrt{x'^2+\gamma^2y^2}-x'}}{\sqrt{x'^2+\gamma^2y^2}}, \tag{11.9}$$

$$\tau_{yz} = \frac{A\mu\gamma}{4}\left(\frac{1}{2\sqrt{x'+i\gamma y}} + \frac{1}{2\sqrt{x'-i\gamma y}}\right) = \frac{A\mu\gamma}{4\sqrt{2}}\frac{\sqrt{\sqrt{x'^2+\gamma^2y^2}+x'}}{\sqrt{x'^2+\gamma^2y^2}}. \tag{11.10}$$

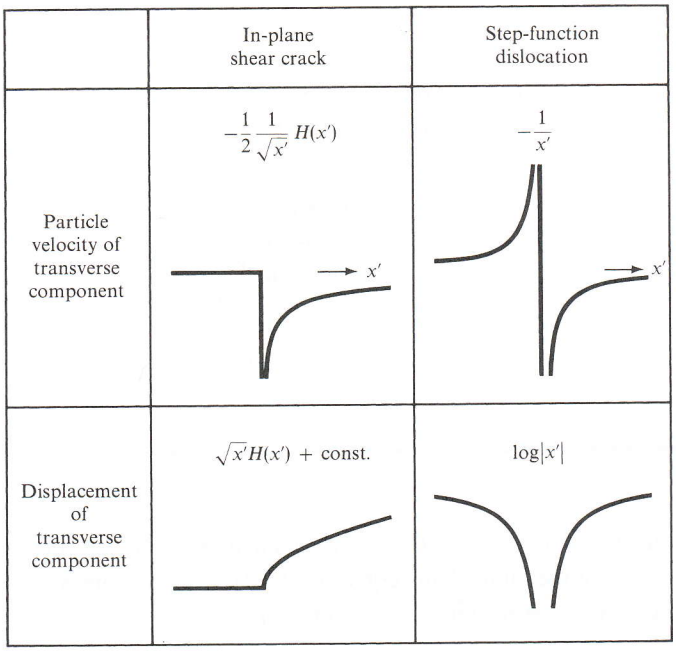

FIGURE **11.3**
Particle velocity and displacement normal to the fault plane for a shear crack and for a step-function shear dislocation.

In contrast to the case of a step-function dislocation, the peak amplitude of particle velocity decays with distance from the fault as $1/\sqrt{y}$. The motion for the crack is smoother than for a dislocation. Before discussing the difference in their spectra, we shall point out a drastic difference in the transverse component of particle motion between the in-plane crack and the in-plane step-function dislocation ("transverse" here means "perpendicular to the fault plane").

The transverse component of particle velocity for the in-plane step-function dislocation (corresponding to $\dot{v}(x, 0, t)$ in (10.63)) is of the form $f(x', y) = 1/x'$ along $y = 0$. Using (11.8), the corresponding solution for the crack is (see Fig. 11.3)

$$g(x', 0) = \frac{1}{2}\int_{-\infty}^{0} \frac{1}{\sqrt{-\xi}}\frac{d\xi}{x' - \xi} = -\frac{1}{2}\frac{1}{\sqrt{x'}} \qquad x' > 0$$

$$= 0 \qquad x' < 0,$$

which has the same form as the shear stress τ_{xy} of the in-plane crack obtained earlier. Remarkably, the transverse component of particle velocity is zero inside the crack. The corresponding displacement will then be constant inside the crack, and of the form $\sqrt{x'}$ ahead of the crack. In the case of step-function slip, the transverse component of displacement shows a symmetric impulsive form ($\sim \log|x'|$), as can be seen in Figure 11.3, which qualitatively agrees with the observed form for the Parkfield earthquake, as discussed in Section 10.2.1. The solution for the crack, on the other hand, does not show the symmetric impulsive form, but an asymmetric step-like form, $\sqrt{x'}\,H(x') + \text{constant}$, as shown in Figure 11.3.

Equation (11.8) shows that $g(x, y)$ is the convolution of $f(x, y)$ with $\frac{1}{2}H(-x)/\sqrt{-x}$. For $k = \omega p > 0$, the Fourier transform of the latter function can be obtained as

$$\begin{aligned}
\frac{1}{2}\int_{-\infty}^{0} \frac{1}{\sqrt{-x}} e^{-ikx}\, dx &= \frac{1}{2}\int_{-i\infty}^{0} \frac{1}{\sqrt{-x}} e^{-ikx}\, dx && \text{(changing the path to the negative imaginary } x\text{-axis)} \\
&= \tfrac{1}{2} e^{i\pi/4} \int_{0}^{\infty} \frac{1}{\sqrt{y}} e^{-ky}\, dy && \text{(putting } x = -iy\text{)} \\
&= e^{i\pi/4} \int_{0}^{\infty} e^{-kz^2}\, dz && \text{(putting } y = z^2\text{)} \\
&= \frac{1}{2}\sqrt{\frac{\pi}{k}} e^{i\pi/4} = \frac{1}{2}\sqrt{\frac{\pi}{\omega p}} e^{i\pi/4}.
\end{aligned}$$

In the frequency domain, therefore, $g(x, y)$ (the seismic motion caused by a propagating semi-infinite crack) has an amplitude spectrum proportional to $1/\sqrt{\omega}$ times the spectrum of $f(x, y)$ (the seismic motion caused by a propagating dislocation with step-function slip), and the phase is shifted by $\pi/4$. This phase shift in the x-coordinate corresponds to a delay of $\pi/4$ in the time axis. Because the $1/\sqrt{\omega}$ factor will attenuate higher frequencies, the motion caused by the propagating crack is smoother than the motion caused by the propagating dislocation with step-function slip.

11.1.2 ENERGETICS AT THE CRACK TIP

As the crack tip propagates, slip occurs across the fault plane. Neglecting friction, the traction on the fault plane is zero over the part where slip is occurring. It seems, therefore, that there is no work done on a crack except for the work against friction. A closer look, however, reveals that a finite amount of work is indeed done at the crack tip per unit distance of its propagation. Since the crack tip is moving, it is not obvious how to calculate this work. Let us first derive a general formula for two-dimensional cracks following Freund (1972). To obtain compact equations we shall use x_i $(i = 1, 2, 3)$ coordinates, put the crack plane at $x_2 = 0$, and let its tip propagate toward the $+x_1$-direction with velocity v. As shown in Figure 11.4, we consider an external surface S_e fixed to the solid body, with the crack surface S_c already formed and an internal surface S_t enclosing and traveling with the crack tip.

In the volume V bounded by these three surfaces, the body obeys the equation of motion, Hooke's law, and strain–displacement relations:

$$\rho \ddot{u}_i = \tau_{ij,j}, \qquad \tau_{ij} = c_{ijkl} e_{kl}, \tag{11.11}$$

$$e_{ij} = \tfrac{1}{2}(u_{i,j} + u_{j,i}), \tag{11.12}$$

where c_{ijkl}, τ_{ij}, e_{ij}, and u_i are the elastic moduli and components of stress, strain, and displacement. We assume that body forces are absent.

On the surfaces S_e and S_t, traction T_i is given as $T_i = \tau_{ij} n_j$, where n_j is the outward normal of the surface of V.

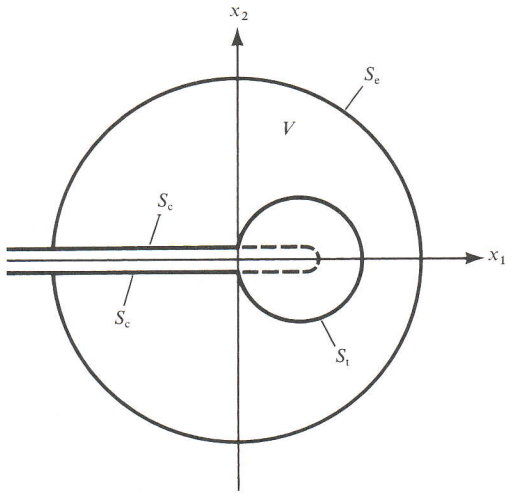

FIGURE **11.4**

The rate of work of the tractions on S_e, and the rates of increase of kinetic energy and strain energy in V, are, respectively,

$$\dot{W} = \int_{S_e} T_i \dot{u}_i \, dS, \qquad \dot{K} = \frac{d}{dt} \int_V \tfrac{1}{2} \rho \dot{u}_i \dot{u}_i \, dV, \qquad \dot{U} = \frac{d}{dt} \int_V \tfrac{1}{2} \tau_{ij} e_{ij} \, dV. \quad (11.13)$$

The energy flow g into the crack tip can now be obtained as a limit of the flow into the inside of S_t:

$$g = \dot{W} - \lim_{S_t \to 0} [\dot{K} + \dot{U}].$$

Since S_t is moving along with the crack tip, the region V in equation (11.13) is time-dependent. Thus both $\dot{K}$ and $\dot{U}$ consist of the change in energy occurring inside V and the flux of energy through the boundary S_t. These contributions are

$$\dot{K} = \int_V \rho \dot{u}_i \ddot{u}_i \, dV + \int_{S_t} \tfrac{1}{2} \rho \dot{u}_i \dot{u}_i v_n \, dS,$$

$$\dot{U} = \int_V \tau_{ij} \dot{u}_{i,j} \, dV + \int_{S_t} \tfrac{1}{2} \tau_{ij} u_{i,j} v_n \, dS \qquad (\text{using } \tau_{ij} = \tau_{ji}),$$

where v_n is the normal component of velocity of a point on S_t. Replacing the first integrand for $\dot{U}$ by $(\tau_{ij}\dot{u}_i)_{,j} - \tau_{ij,j}\dot{u}_i$ and applying the divergence theorem to $\int_V (\tau_{ij}\dot{u}_i)_{,j} \, dV$, we find

$$\begin{aligned} g = & \int_{S_e} T_i \dot{u}_i \, dS - \lim_{S_t \to 0} \left[\int_V (\rho \dot{u}_i \ddot{u}_i - \tau_{ij,j} \dot{u}_i) \, dV + \int_{S_e + S_c} \tau_{ij} n_j \dot{u}_i \, dS \right. \\ & \left. + \int_{S_t} \left(\tau_{ij} n_j \dot{u}_i + \tfrac{1}{2} \tau_{ij} u_{i,j} v_n + \tfrac{1}{2} \rho \dot{u}_i \dot{u}_i v_n \right) dS \right] \qquad (11.14) \\ = & - \lim_{S_t \to 0} \int_{S_t} \left(\tau_{ij} n_j \dot{u}_i + \tfrac{1}{2} \tau_{ij} \dot{u}_{i,j} v_n + \tfrac{1}{2} \rho \dot{u}_i \dot{u}_i v_n \right) dS, \end{aligned}$$

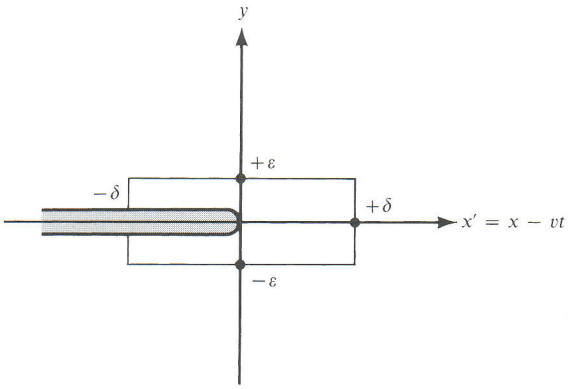

FIGURE **11.5**

where we used (11.11) and (11.12). The contribution from S_c is zero because $v_n = 0$ and because the crack surface is traction-free. (As mentioned in the beginning of this section, we chose to neglect the effect of friction here.)

Now, coming back to the coordinate frame (x', y) moving with the tip, we shall choose a rectangular surface shown in Figure 11.5 as S_t. The side lengths of the rectangle are 2δ in the x-direction and 2ε in the y-direction. If we shrink the width ε to zero, the contribution from the sides $x = \pm\delta$ is zero. Since v_n is zero on the sides $y = \pm\varepsilon$, equation (11.14) is simplified to

$$g = \lim_{\delta \to 0} \int_{-\delta}^{\delta} \mathbf{T}(x', 0) \cdot \left[\dot{\mathbf{u}}(x', +0) - \dot{\mathbf{u}}(x', -0)\right] dx'.$$

Thus, by putting equation (11.6) into the above integral, the rate of work for the anti-plane case is obtained as

$$g = \frac{AvK}{2\sqrt{2\pi}} \lim_{\delta \to 0} \int_{-\delta}^{\delta} \frac{H(-x')}{\sqrt{-x'}} \frac{H(x')}{\sqrt{x'}} dx'$$

and, using equation (11.7) for the in-plane case, as

$$g = \frac{A'vK'}{2\sqrt{2\pi}} \lim_{\delta \to 0} \int_{-\delta}^{\delta} \frac{H(-x')}{\sqrt{-x'}} \frac{H(x')}{\sqrt{x'}} dx'.$$

The integrand in the above formulas is zero except at $x' = 0$, yet the integration gives a finite result because the integrand behaves like a Dirac delta function. To show this, let us consider the following integral:

$$\int_{-\infty}^{\infty} \frac{H(x')H(x - x')}{\sqrt{x'}\sqrt{x - x'}} dx' = \int_{0}^{x} \frac{dx'}{\sqrt{x'}\sqrt{x - x'}} = \pi H(x) \qquad \text{(see Box 9.3).}$$

It then follows that

$$\int_{-\infty}^{\infty} \frac{H(x')}{\sqrt{x'}} \frac{H(-x')}{\sqrt{-x'}} dx' = \pi H(0) = \frac{\pi}{2}.$$

Thus, for the anti-plane crack, the rate of work done at the crack tip is

$$g = \sqrt{\frac{\pi}{2}}\frac{AvK}{4} = \frac{vK^2}{2\mu}\Big/\sqrt{1-\frac{v^2}{\beta^2}}, \tag{11.15}$$

and for the in-plane crack

$$g = \frac{v}{8}\frac{v^2K'^2}{\mu\beta^2}\left[\sqrt{1-\frac{v^2}{\alpha^2}} - \left(1-\frac{v^2}{2\beta^2}\right)^2\Big/\sqrt{1-\frac{v^2}{\beta^2}}\right]^{-1}. \tag{11.16}$$

The above result may be obtained without using a value of $H(x)$ at $x = 0$. From equations (11.9) and (11.12) for stress and particle velocity of the anti-plane crack, the first term of the integrand of (11.14) is given by

$$2\tau_{yz}(x', y)\dot{w}(x', y) = \frac{vK^2y}{2\pi\mu(x'^2 + \gamma^2y^2)},$$

where K is the stress-intensity factor defined earlier and $\gamma = \sqrt{1 - v^2/\beta^2}$. Putting $y = \pm\varepsilon$ into the above formula and integrating from $x' = -\delta$ to $x' = +\delta$, we get

$$g = \lim_{\varepsilon\to 0}\lim_{\delta\to 0}\frac{vK^2}{\pi\mu\gamma}\tan^{-1}\left(\frac{\varepsilon}{\delta\gamma}\right) = \frac{vK^2}{2\mu\gamma}, \tag{11.17}$$

which confirms the result given in (11.15).

In the case of the anti-plane crack, the energy flow at the tip is zero when $K = 0$, i.e., when the rupture velocity is equal to the shear velocity. In the case of the in-plane crack, it is zero when the rupture velocity is equal to the Rayleigh-wave velocity. Thus, at these velocities, energy needed for creating new surfaces of the crack cannot be supplied to the crack tip. In this sense, they are the terminal velocities of crack propagation. Equation (11.16) shows that if the rupture velocity exceeds the Rayleigh-wave velocity, g becomes negative. In other words, the crack tip becomes a source of energy flow instead of a sink. This is physically unacceptable, and it appears that the speed of the in-plane shear crack cannot exceed the Rayleigh-wave velocity. This conclusion, however, will be modified in Section 11.2.3, where we discuss rupture propagation in a medium with finite cohesive force.

11.1.3 COHESIVE FORCE

The solutions for stress and particle velocity around the propagating crack tip obtained in Section 11.1.1 are still not realistic, because they both become infinite at the crack tip. All materials have a finite strength and cannot withstand stress beyond some limit. The way to eliminate the singularities is found by using the concept of *cohesive force*, introduced by Barenblatt (1959). This force is distributed inside the crack near the tip, and it opposes the external stress.

BOX **11.2**
Fracture criteria

Since most materials fracture when stressed beyond some critical level, it is natural to describe the condition for fracture by a critical applied stress, or strength of material. It practice, however, it has long been known that the fracture strength of a given material varies greatly. The theories built around the concept of strength as a material constant were for a long time incapable of accounting for observed diversity in fracture behavior.

A breakthrough was made by A.A. Griffith in 1920. He assumed the existence of flaws in material in the form of cracks. Creating new crack surfaces requires an increase of the free surface energy. This energy must be supplied from the surrounding medium for the crack to extend. Griffith's fracture criterion is based on the balance of consumed surface energy and the supply of mechanical energy for an infinitesimal virtual increase in crack length. In this section, we have just calculated the rate of supply of mechanical energy to the crack tip when the crack tip moves at a constant speed ((11.15) and (11.16)). In Section 11.2.1, we shall use the Griffith concept of energy balance in deriving the equation of motion for a crack tip, equation (11.34).

An alternative approach to fracture mechanics was formulated around the concept of stress-intensity factor by G. R. Irwin and his associates in about 1950. It was found that the Griffith fracture criterion is equivalent to the existence of a critical stress-intensity factor. If the stress-intensity factor exceeds the critical value, the crack will extend. We shall call this the Irwin criterion.

In equation (11.15) and (11.16), we have shown that the energy flow into the crack tip is determined by the stress-intensity factor K or K', and the rupture-propagation velocity v. Therefore, at the initiation of crack extension, when $v = 0$, the energy flow and stress-intensity factor are uniquely related, demonstrating the equivalence of Griffith and Irwin criteria. The equivalence relation is shown explicitly in (11.22), setting $v = 0$ there for an anti-plane crack and also in (11.82) for an in-plane crack.

For a finite rupture velocity v, both the Griffith surface energy and the critical stress-intensity factor may depend on v. In Sections 11.2.2 and 11.2.3, we shall consider two fracture criteria. In the Griffith criterion, we assume that the surface energy does not depend on v; in the Irwin criterion, we assume that the critical stress intensity factor is independent of v. Figure 11.21 compares the motion of the crack tip obtained by the two criteria.

Let us consider the case of an anti-plane crack, and put the total traction on the ruptured surface ($x' \leq 0$) as

$$\sigma_{yz}(x', 0) = \sigma_{yz}^{\mathrm{d}} + \sigma_{\mathrm{c}}(x'). \tag{11.18}$$

Here σ_{yz}^{d} is due to dynamic friction and acts all over the crack, but the cohesive force (per unit area) $\sigma_{\mathrm{c}}(x')$ is nonzero only in $-d < x' \leq 0$, where d is the length of the end region, as shown in Figure 11.6. The distribution of the cohesive force will generate a concentration of τ_{yz} ahead of the crack tip, with the stress-intensity factor given by

$$-\sqrt{\frac{2}{\pi}} \int_{-d}^{0} \frac{\sigma_{\mathrm{c}}(\xi)}{\sqrt{-\xi}}\, d\xi. \tag{11.19}$$

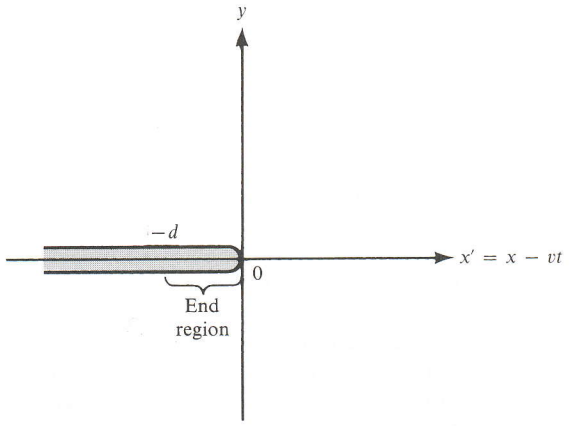

FIGURE **11.6**

This result is derived later in Box 11.3, in a discussion of equation (11.55). The original stress singularity due to the external stress may be eliminated if we choose the cohesive force $\sigma_c(\xi)$ that satisfies the condition

$$K = \sqrt{\frac{2}{\pi}} \int_{-d}^{0} \frac{\sigma_c(\xi)}{\sqrt{-\xi}}\, d\xi. \tag{11.20}$$

With this choice of $\sigma_c(\xi)$, the stress component $\sigma_{yz}(x', 0)$ will be finite and continuous at the crack tip. Since the slip velocity $\Delta\dot{w}$ is the Hilbert transform of the shear stress times a constant, as shown in equation (11.3), the singularity of $\Delta\dot{w}$ is also removed if the shear stress becomes continuous there.

If d is small, the elastic field due to the cohesive force is limited near the crack tip and does not affect the field outside the immediate vicinity of the crack tip. Then the energy flow into the crack tip through the external surface will be the same as given in (11.15) for the case of no cohesive force. This energy flow is absorbed to create a new surface of the crack. Expressing the surface energy per unit area as G, we have

$$g = 2Gv, \tag{11.21}$$

where the factor 2 accounts for both faces of the crack. From (11.15) and (11.21), we find

$$G = \frac{K^2}{4\mu} \Big/ \sqrt{1 - \frac{v^2}{\beta^2}} \tag{11.22}$$

(A similar relation may be obtained for an in-plane shear crack using (11.16).)

In order to get a rough estimate of the highest frequencies involved in seismic motion caused by propagation of a crack, we shall assume that the cohesive force is uniformly distributed over the end region. The corresponding stress-intensity factor is

$$K = \sqrt{\frac{2}{\pi}} \int_{-d}^{0} \frac{\sigma_c}{\sqrt{-\xi}}\, d\xi = \frac{2\sigma_c}{\sqrt{\pi}} \sqrt{2d}, \tag{11.23}$$

where σ_c is the cohesive force per unit area. Putting (11.23) into (11.22), we find

$$G = \frac{2\sigma_c^2 d}{\mu\pi} \Big/ \sqrt{1 - \frac{v^2}{\beta^2}}. \tag{11.24}$$

This is a relationship between important quantities that determine the seismic motion around the crack tip, about which we know very little. In general, G, σ_c, and d may depend on the rupture velocity.

Since d is the measure of distance over which slip is resisted, the larger d is, the slower the slip at the initial stage of faulting. Contrarily, we expect higher slip velocity and acceleration as d gets shorter. The characteristic time constant t_d may be given by d/v:

$$t_d = d/v = \frac{\pi\mu G\sqrt{1 - (v^2/\beta^2)}}{2\sigma_c^2 v}. \tag{11.25}$$

t_d is the time constant that controls the high end of the seismic spectrum. Static experiments on rock samples in the laboratory give G on the order of 10^3 erg/cm^2 and σ_c on the order of 10^9 dyn/cm^2. For a rough estimate, we shall assume that their order of magnitude remains the same in the dynamic case, so that for $\beta = 3.5$ km/s, $v = 3$ km/s, and $\mu = 3 \times 10^{11}$ dyn/cm^2, we get

$$t_d = 10^{-9}\text{s}.$$

Thus we expect radiation of seismic waves with frequency up to a gigahertz if the laboratory values are applicable.

In the actual field situation, G may increase with crack length. The stress around the crack tip increases as the crack length increases. (As shown in Box 11.1, the static stress-intensity factor increases for larger cracks.) Consequently, the volume of the region of microcracks and plastic deformation will increase. This region will absorb energy, making the apparent value of G greater for larger earthquakes.

The highest frequency contained in usual earthquake records is on the order of 100 Hz. Assuming that the cohesive stress σ_c in the actual fault gouge is on the order of 10^8 dyn/cm^2, the value of G corresponding to $t_d = 0.01$ s will be around 10^8 erg/cm^2 from (11.25), which is many orders of magnitude greater than the laboratory values.

The physical meaning of cohesive force becomes clearer if we write it, instead of equation (11.18), in the form of constitutive equations, such as

$$\sigma_{yz}(x', 0) = \sigma_{yz}^{\text{d}} + \sigma_c[\Delta w(x')] \qquad x' \le 0 \tag{11.26}$$

or

$$\sigma_{yz}(x', 0) = \sigma_{yz}^{\text{d}} + \sigma_c[\varepsilon(x')] \qquad x' \le 0, \tag{11.27}$$

where ε is the plastic strain in the fault gouge and Δw is the equivalent slip between the fault surfaces corresponding to the plastic strain. If the thickness of the fault gouge is b, we may take $\Delta w = b\varepsilon$. The specific surface energy G can be expressed as $G = \frac{1}{2}\int_0^\infty \sigma_c(D)\, dD$,

where the factor $\frac{1}{2}$ accounts for the two surfaces of the crack. Relation (11.27) may be determined by laboratory experiments on the stress–strain relation of rock samples and field studies of gouge thickness, and it may be appropriate to allow σ_c to depend on $\Delta\dot{w}$ as well as on Δw. Once the relation is known, the slip function can be calculated by an iterative method. We start with an initial guess of the slip function $\Delta w(x')$ and obtain the corresponding cohesive force from (11.26) or (11.27). Then we can calculate the stress-intensity factor K from (11.20). At a distance sufficiently far from the tip compared with the scale of the end region, the cohesive force no longer governs the slip function, which is determined instead by macroscopic crack parameters such as the shape, length, and stress drop. Knowing σ_{yz} for $-\infty < x' < \infty$, the slip velocity can be obtained by the Hilbert transform (see equation (11.3)). The resulting slip function can be used as the second trial function for revising the cohesive force. The iteration proceeds until the slip function converges to a final solution. Ida (1972, 1973) used this method to calculate the slip function and its time derivatives for various cases of the cohesive force diagram (σ_c as a function of slip [Δw]), assuming a semi-infinite crack with constant stress drop as the macroscopic model, and discussed the maximum acceleration and velocity in terms of this material property. Andrews (1976) extended Ida's work and incorporated the cohesive force in a finite-difference calculation of crack propagation (discussed in Section 11.2.3 and Fig. 11.26), combining numerical analysis of rupture propagation with laboratory results on rock mechanics.

11.1.4 NEAR FIELD OF A GROWING ELLIPTICAL CRACK

In Section 10.1.6, we studied the far-field body waves from an elliptical crack growing with constant velocity and keeping the same shape. Neglecting the stopping phase, we found that the initial rise of far-field displacement grows parabolically, being proportional to the square of time measured from the onset. The corresponding acceleration showed a finite discontinuity at the onset. In this section, we shall consider seismic motion in the near field of the growing elliptical crack, for which a Cagniard solution is available.

Let us assume initially a state of uniform stress $\boldsymbol{\sigma}^0$ and suppose that a plane shear crack nucleates at the origin at time $t = 0$. The fault surface $S(t)$ is defined in Cartesian coordinates by the ellipse

$$S(t) = \left\{ x_3 = 0 \colon x_1^2/u^2 + x_2^2/v^2 \le t^2 \right\},$$

which (see Figure 11.7)) has axes growing steadily at speeds u and v, each less than (or equal to) the shear-wave speed β. The shear stresses across plane $x_3 = 0$ are influenced by waves emanating from the point of nucleation, but after arrival of the rupture they drop to new values prescribed over $S(t)$.

To describe the problem further, let $\mathbf{u}$ be displacement from the initial (prestressed, static) position, with $\boldsymbol{\tau}$ as the stress tensor due to $\mathbf{u}$ (so that $\boldsymbol{\sigma}^0 + \boldsymbol{\tau}$ is the total stress). Within an infinite homogeneous medium, $\mathbf{u}$ and $\boldsymbol{\tau}$ have certain symmetric properties with respect to the crack plane $x_3 = 0$ (see Problem 10.2): from equation (10.39) or an argument similar to the one used in the in-plane problem (Section 10.2.4), we find that τ_{33}, u_1, and u_2 are odd functions of x_3 when the discontinuity across the crack plane is restricted to

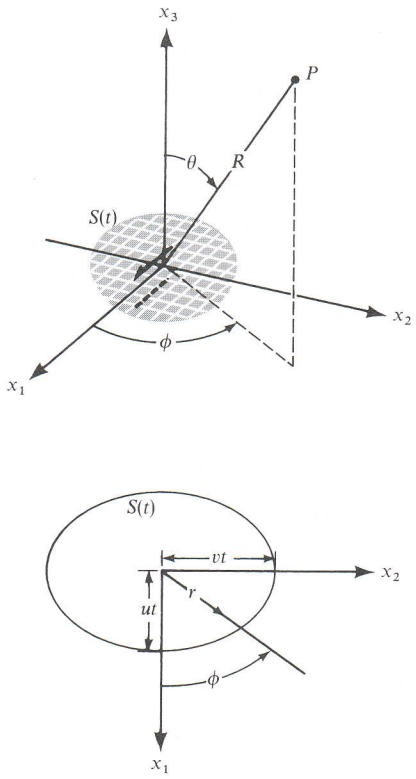

FIGURE **11.7**

shearing. These quantities must therefore be zero at $x_3 = 0$ wherever they are continuous there. Thus we have the following boundary conditions:

$$\tau_{33} = 0 \qquad \text{everywhere on} \quad x_3 = 0 \tag{11.28}$$

and

$$u_1 = u_2 = 0 \qquad \text{on} \quad x_3 = 0 \quad \text{but off } S(t). \tag{11.29}$$

Burridge and Willis (1969) found the following simple solution for the slip function across a growing elliptical shear crack:

$$\begin{aligned} \begin{pmatrix} u_1 \\ u_2 \end{pmatrix} &= \begin{pmatrix} a \\ b \end{pmatrix} \sqrt{t^2 - \frac{x_1^2}{u^2} - \frac{x_2^2}{v^2}} \qquad \text{on } x_3 = +0 \text{ and } S(t) \\ &= \begin{pmatrix} 0 \\ 0 \end{pmatrix} \qquad \text{on } x_3 = +0 \text{ but off } S(t). \end{aligned} \tag{11.30}$$

The elastic field generated by this slip function under the conditions (11.28) and (11.29) indeed gives a shear-stress jump (τ_{13}, τ_{23}) that is constant in time and space on $S(t)$; τ_{13} is proportional to a and τ_{23} is proportional to b, where a and b are particle-velocity components

at the center of the crack, as can be seen from (11.30). For simplicity, we shall take the x_1-axis in the direction of maximum initial shear, so that no drop occurs in the stress component τ_{23}. In this case, $b = 0$ and the slip component u_2 disappears. On the moving part of the fault, τ_{13} is constant, and we can think of the total shear stress $\sigma_{13}^0 + \tau_{13}$ as being proportional to σ_{33}^0 via a dynamic coefficient of friction according to the Coulomb law of friction.

Following Richards (1973b, 1976a), we shall take the following steps for computing the elastic field radiated from the growing crack:

(i) Fourier transformation for x_1 and x_2; Laplace transformation for t:

$$f(x_1, x_2, x_3, t) \rightarrow f(k_1, k_2, k_3, s)$$

where f is any dependent variable (such as a displacement component) of interest. Boundary conditions on $x_3 = 0$ are thus transformed to

$$\tau_{33} = 0, \qquad u_1 = \frac{4\pi auv}{(s^2 + k_1^2 u^2 + k_2^2 v^2)^2}, \qquad u_2 = 0.$$

(ii) Transformation of the wave equation and use of potentials to derive algebraic expressions for $\mathbf{u}(k_1, k_2, x_3, s)$. The double Fourier inverse transform is taken, yielding the forward Laplace transform as an explicit double integral over the whole (k_1, k_2) plane. A rotation and stretch of the (k_1, k_2) plane to variables (w, q) is carried out via the de Hoop transformation

$$k_1 = (s/\alpha)(q \cos\phi - w \sin\phi),$$
$$k_2 = (s/\alpha)(q \sin\phi + w \cos\phi),$$

where α is the P-wave speed. The Laplace-transformed P-wave component of displacement at position $\mathbf{x}$ then has the form

$$\mathbf{u}^P(\mathbf{x}, s) = (1/s^2) \int_0^\infty dw \int_{-\infty}^\infty dq\, \mathbf{F}(q, w, \phi) e^{-st}, \tag{11.31}$$

where $\mathbf{F}$ is known, $t = t(q, w, \theta) \equiv \left[-iq \sin\theta + \sqrt{1 + q^2 + w^2} \cos\theta\right] (R/\alpha)$, and the spherical polars (R, θ, ϕ) for $\mathbf{x}$ are shown in Figure 11.7. It can be shown that only the positive real q-axis is needed for the integration in (11.31). There is a similar expression for the S-wave component.

(iii) Application of Cagniard's method, turning the q-integral into the Laplace transform of the w-integral, so that displacement in the time domain is recognized as a single integral over w. A complication arises because of singularities of the integrand $\mathbf{F}$, as shown in Figure 11.8. This is a diagram of the complex q-plane, and it shows that between the real-axis path of integration needed in (11.31) and the Cagniard path (on which the exponent $t(q, w, \theta)$ in (11.31) is real), the integrand has a pole. It turns

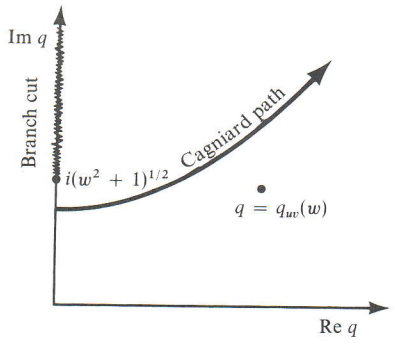

FIGURE **11.8**
There is a pole at q_{uv} near the Cagniard path for evaluating (11.31). [From Richards, 1976a.]

out to be a second-order pole, denoted by q_{uv}, and is due to the moving nature of the source. It is necessary to pick up residues in converting to the Cagniard path, giving the form

$$\mathbf{u}^P(\mathbf{x}, s) = \frac{1}{s^2}\int_0^\infty dw \int_0^\infty dt\, \mathbf{F}(q(t), w, \phi)e^{-st}\frac{dq}{dt} + \int_0^\infty dw\, \mathbf{R}(q_{uv}, w, \phi, s)e^{-st}(q_{uv}, w, \theta), \tag{11.32}$$

From the first term on the right-hand side here, one can invert to the time domain in the usual fashion (i.e., by reversing the order of integration and recognizing the result as a forward Laplace transform), obtaining a single integral over w. The second term on the right-hand side of (11.3) is already in the form suitable for recognition as the Laplace transform of a function of time. This term therefore results in an algebraic closed-form expression. This overall method, an algebraic expression resulting from an integral of residues, was first developed by Gakenheimer and Miklowitz (1969) for solving Lamb's problem with a moving source.

As usual for Cagniard inversion of three-dimensional problems (see Section 6.5), the complete seismogram can be calculated only numerically, an integration being necessary for each point in the time series. Figure 11.9 shows theoretical record sections for x_1- and x_3-components of acceleration near a left-lateral strike-slip fault. The coordinates for the four stations are (1, 1.5, 0.5), (4, 1.5, 0.5), (7, 1.5, 0.5), and (10, 1.5, 0.5). The density of the medium is 2.7 gm/cm^3, the P-wave velocity is 5.2 km/s, and the S-wave velocity is 3 km/s. The rupture speed in the x_1-direction is 90% of the Rayleigh-wave velocity, and that in the x_2-direction is 90% of the S-wave velocity. We see, in this case, small P-waves, sharp step-like S-waves arriving from the nucleation point, and large acceleration associated with the passage of the crack tip. The amplitude of waves from the nucleation point decreases with distance, whereas the acceleration associated with passage of the crack tip increases because the stress-intensity factor increases with increasing crack length.

The corresponding displacement records are shown in Figure 11.10. As discussed in Section 11.1.1, the transverse component shows a step-like waveform rather than a

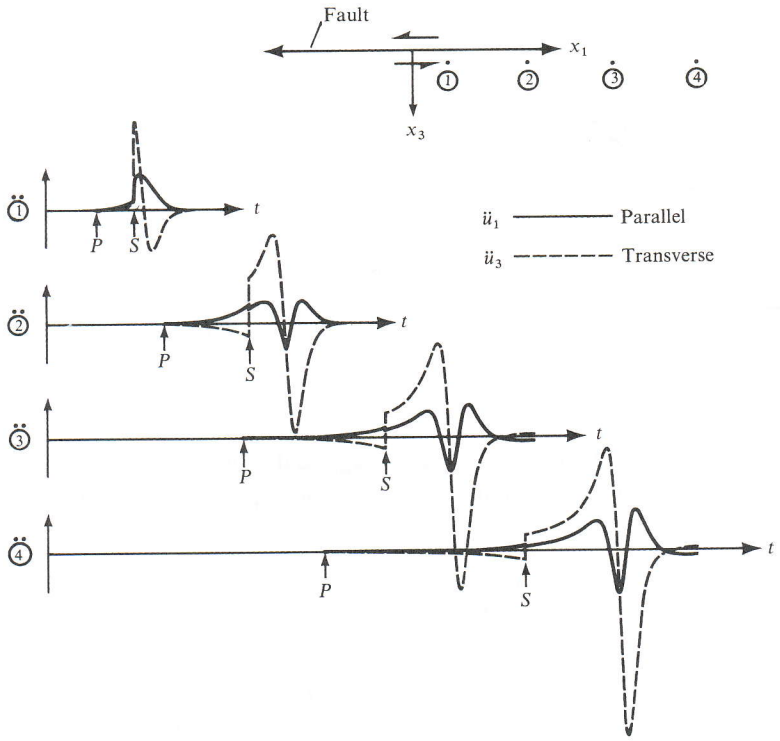

FIGURE **11.9**
Synthetic seismograms for x_1- and x_3-components of acceleration at stations shown at the top. [From Richards, 1976a.]

symmetric, impulsive form. The parallel components show a very slow rise beginning at the arrival of P-waves from the nucleation point, and do not show any clear feature that can be associated with passage of the rupture front. This shows the difficulty of accurately estimating rupture velocity from displacement measurements at points off the crack plane.

Compact formulas can be obtained for approximate waveforms corresponding to the arrivals of P- and S-waves from the nucleation point. At the arrival time $t = R/\alpha$, we find that the acceleration has a jump discontinuity:

$$\ddot{\mathbf{u}}^P = \frac{4u\upsilon\beta^2 \cos\theta \sin\theta}{\alpha^3(1 - D\sin^2\theta)^2}\, a \cos\phi\, \frac{H(t - R/\alpha)}{R}\hat{\mathbf{R}},$$

where $D = (u^2 \cos^2\phi + \upsilon^2 \sin^2\phi)/\alpha^2$. (R, θ, ϕ) are the spherical coordinates shown in Figure 11.7. The vector $\ddot{\mathbf{u}}^P$ points to the radial (i.e. longitudinal) direction from the nucleation point, given by the unit vector $\hat{\mathbf{R}}$. The acceleration due to shear waves from the nucleation point shows a jump discontinuity at $t = R/\beta$:

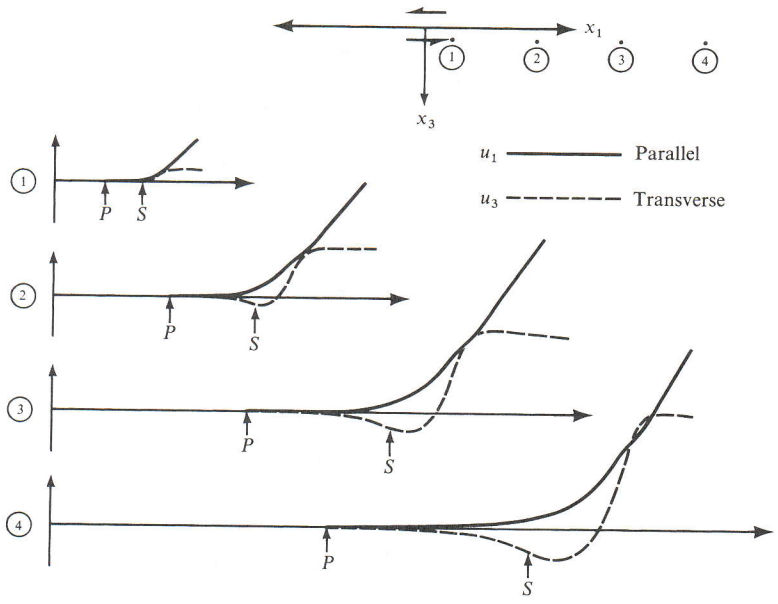

FIGURE **11.10**
Synthetic seismograms for x_1- and x_3-components of displacement at stations shown at the top. [From Richards, 1976a.]

$$[\ddot{u}_1^S, \ddot{u}_2^S, \ddot{u}_3^S] = \frac{2uv}{(1 - D\alpha^2 \sin^2\theta/\beta^2)^2} \left[\cos\theta\ (a, 0, 0)\right.$$
$$\left. -a \sin\theta \cos\phi\ (\sin 2\theta \cos\phi, \sin 2\theta \sin\phi, \cos 2\theta)\right] \frac{H(t - R/\beta)}{R}.$$

The high-frequency asymptote of the acceleration is therefore proportional to ω^{-1}, and the corresponding displacement spectrum has a high-frequency asymptote like ω^{-3}, in agreement with previous results (equation (10.30)). The radiation pattern of these waves shows a double-couple symmetry modified by the factors $(1 - D \sin^2\theta)^{-2}$ for P-waves and $(1 - D\alpha^2 \sin^2\theta/\beta^2)^{-2}$ for S-waves.

Another compact form of approximate solution can be obtained for singularities of particle velocity and traction components near the crack tip. Let us denote the arrival time of the crack tip at $(x_1, x_2, 0)$ as t_c, so that

$$t_c = \sqrt{x_1^2/u^2 + x_2^2/v^2}.$$

The particle velocity $\dot{u}_1$ on the plane $x_3 = 0$ is given by boundary conditions (11.29) and (11.30) as

$$\dot{u}_1 \sim a\sqrt{t_c/2}\, H(t - t_c)/\sqrt{t - t_c}. \tag{11.33}$$

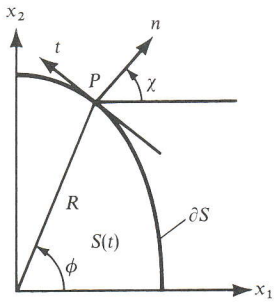

FIGURE **11.11**
Local Cartesian coordinates in the normal (n) and tangent (t) directions. [From Richards, 1976a.]

Singularities in $\dot{u}_2$ and τ_{33} are absent on $x_3 = 0$, since these quantities are zero throughout the plane. Singularities in the remaining velocity and traction components on $x_3 = 0$ are

$$\dot{u}_3 \sim \frac{2\beta^2 V a \cos\phi}{U\alpha^2 B_S}\left[\tfrac{1}{2}\alpha^2/\beta^2 + B_S^2 - B_P B_S\right]\sqrt{\frac{t_c}{2F}}\,\frac{H(t_c - t)}{\sqrt{t_c - t}},$$

$$\tau_{13} \sim \frac{4\mu\beta^2 a}{U^2\alpha^3 F B_S}\left[\left(B_P - B_S\right)B_S V^2\cos^2\phi + \tfrac{1}{4}\left(U^2 B_S^2 F - V^2\cos^2\phi\right)\left(\alpha^2/\beta^2\right)\right] \tag{11.34}$$

$$\times\sqrt{t_c/2}\,H(t_c - t)/\sqrt{t_c - t},$$

$$\tau_{23} \sim \frac{4\mu\beta^2 a\cos\phi\sin\phi}{\alpha^3 F B_S}\left[B_S B_P - B_S^2 - \tfrac{1}{4}\left(\alpha^2/\beta^2\right)\right]\sqrt{\frac{t_c}{2}}\,\frac{H(t_c - t)}{\sqrt{t_c - t}},$$

where μ is the rigidity and all capital letter symbols are dimensionless quantities given by

$$U = u/\alpha, \qquad V = v/\alpha, \qquad F = U^2\sin^2\phi + V^2\cos^2\phi,$$

$$B_P^2 + 1 = B_S^2 + \frac{\alpha^2}{\beta^2} = \frac{U^4\sin^2\phi + V^4\cos^2\phi}{U^2V^2F}.$$

Since the singularities (11.33) and (11.34) describe local properties of the motion at points near the crack tip, it is instructive to work with a coordinate system related naturally to the local geometry. Figure 11.11 shows such a system, using directions of the normal, the tangent, and the binormal (i.e., the x_3-axis). Tensor components are rotated to

$$\tau_{3n} = \tau_{31}\cos\chi + \tau_{23}\sin\chi, \qquad \tau_{t3} = -\tau_{31}\sin\chi + \tau_{23}\cos\chi.$$

Letting v_n be the velocity of rupture in direction n, we find that

$$v_n = \frac{uv}{\alpha}\sqrt{\frac{F}{U^4\sin^2\phi + V^4\cos^2\phi}},$$

which is simply related to B_P and B_S.

We can now resolve the local motion into in-plane components (u_n and τ_{zn}) and anti-plane components (u_t and τ_{zt}). Then the singularities for the in-plane components are

$$\dot{u}_n \sim \frac{a v_n V \cos\phi}{\alpha U}\sqrt{\frac{t_c}{2F}}\,\frac{H(t-t_c)}{\sqrt{t-t_c}},$$

$$\tau_{3n} \sim \frac{-a\mu\beta^2 v_n V \mathsf{R}(1/v_n)\cos\phi}{B_S U}\sqrt{\frac{t_c}{2F}}\,\frac{H(t_c-t)}{\sqrt{t_c-t}},$$

where $\mathsf{R}(1/v_n) = [(\alpha^2/\beta^2)(v_n^2/\beta^2) - 4B_S B_P + 4B_S^2]/(\alpha^2 v_n^2)$, so that R is the Rayleigh function of (5.56),

$$\mathsf{R}(p) \equiv \left(\frac{1}{\beta^2} - 2p^2\right)^2 - 4p^2\sqrt{p^2 - \frac{1}{\alpha^2}}\sqrt{p^2 - \frac{1}{\beta^2}}, \tag{11.35}$$

and singularities for the anti-plane components are

$$\dot{u}_t \sim \frac{-a v_n U \sin\phi}{\alpha V}\sqrt{\frac{t_c}{2F}}\,\frac{H(t-t_c)}{\sqrt{t-t_c}},$$

$$\tau_{t3} \sim \frac{-a\mu U v_n B_S \sin\phi}{\alpha^2 V}\sqrt{\frac{t_c}{2F}}\,\frac{H(t_c-t)}{\sqrt{t_c-t}}.$$

In agreement with results obtained in Section 11.1.1, the in-plane stress singularity will vanish wherever the rupture velocity is the Rayleigh-wave velocity, and the anti-plane singularity will be zero wherever the rupture velocity is the shear velocity (then, $B_S = 0$). The energy flow into the crack tip per unit length of rupture front can be obtained in the same way as for the two-dimensional crack. Integrating the work rate over the area enclosing the crack tip and moving with it, we find the rate of energy flow into the crack tip as

$$\begin{aligned} g &= \lim_{\substack{\delta^+\to 0\\ \delta^-\to 0}} \int_{-\delta^-}^{\delta^+} \left(\tau_{3n}\,\Delta\dot{u}_n + \tau_{t3}\,\Delta\dot{u}_t\right) dn \\ &= \frac{\pi\mu\beta^2 v_n}{4\alpha^3 U^2 V^2 B_S F} a^2 t_c \left[B_S^2 \left(v_n/\beta\right)^2 U^4 \sin^2\phi - \mathsf{R}\left(1/v_n\right)\alpha^2 v_n^2 V^4 \cos^2\phi\right]. \end{aligned} \tag{11.36}$$

For v_n less than the Rayleigh-wave speed c_R, $\mathsf{R}(1/v_n)$ is negative and the crack tip is an energy sink of both anti-plane and in-plane motions. But for $v_n > c_R$, $\mathsf{R}(1/v_n)$ is positive and the crack tip becomes the apparent energy source for in-plane motion. This is unrealistic for a pure in-plane crack, but may be possible if the energy flow supplied by the anti-plane component (positive for $v_n < \beta$) can compensate for it (Andrews, 1994). The motion at $\phi = 0$ is purely in-plane, and the terminal velocity of the crack tip will be the Rayleigh-wave velocity c_R. The motion at $\phi = 90°$ is purely anti-plane, with its terminal velocity being the shear-wave velocity β. For arbitrary ϕ, setting $g = 0$ in (11.36) will give the terminal velocity. The resultant terminal crack will be approximately elliptical, with major and minor axes growing at speeds β and c_R.

The above discussion of terminal velocity is based only on the rates of energy balance at the crack tip. In the case of an in-plane shear crack, it is possible that the stress associated with P- and S-waves running ahead of the crack tip can overcome the cohesive force (if finite), and the rupture velocity will exceed the Rayleigh-wave velocity, eventually reaching the P-wave velocity. We shall come back to this point in Section 11.2.3.

11.1.5 THE FAR-FIELD SPECTRUM FOR A CIRCULAR CRACK THAT STOPS

So far we have considered only cases in which the crack grows with a constant velocity. The results gave us some insight into the slip function expected for a shear crack and also some understanding of its elastic near field. But to understand its far field, we must solve a more difficult problem in which the growth of the crack is stopped.

Let us consider a circular crack that nucleates at its center at time $t = 0$, expands with a constant velocity v, and suddenly stops at a radius r_c. Up to the time of stopping, $t = r_c/v$, the problem is self-similar and the slip function given in (11.30) for $u = v$ gives the exact solution. If we freeze the motion at this instant, we get the kinematic model depicted in Figure 10.10, for which the compact far-field solution of Sato and Hirasawa (1973) is given in equation (10.27). This freezing of motion is unrealistic, because it violates causality. At the instant of stopping, the points inside the crack have not yet sensed the termination of crack growth. The slip function of another kinematic model, proposed by Molnar *et al.* (1973) and shown in Figure 10.12, is more plausible; and the ramp-function slip at the crack center is quite appropriate, although the slip function at other points should have a square-root rise, as proposed by Boatwright (1980).

The high-frequency asymptote of the far-field displacement spectrum was determined by the form of the slip function in space near the crack tip, as discussed in Section 10.1.6. For the step-function rise, the asymptote is expected to be $\omega^{-3/2}$, and for the square-root rise, ω^{-2}. As discussed in Section 11.1.3, the cohesive force smooths these singularities over the length of the end region. The rupture velocity divided by this length will give the upper limit of frequency to which the asymptote is applicable.

Because of the difficulty in dealing with multiple diffraction at the edges of the crack, no analytic solution is available for the elastic field of a growing crack that stops. Burridge (1969) used a numerical solution of the integral-equation representation of the problem to solve some finite in-plane and anti-plane cracks. A similar method, originated by Hamano (1974), has been used by Das and Aki (1977a). Finite-difference or finite-element methods have also been used for similar problems by Hanson *et al.* (1971), Dieterich (1973), and Andrews (1975). Here we shall outline the work of Madariaga (1976), who used a finite-difference method to calculate the far-field seismic spectrum from a growing circular crack that stops. As we shall see in his results, the finite mesh size and some smoothing procedures introduce an artificial end region similar to that due to cohesive force.

We shall use the same notation and coordinate system as for the elliptical crack in Section 11.1.4 (Fig 11.7). We shall again assume that the stress drop on the crack occurs only in the τ_{13} component. Similarly, τ_{33} is zero on the plane $x_3 = 0$, and u_1 and u_2 are zero outside the crack on the plane $x_3 = 0$. The boundary conditions on $x_3 = 0$ are therefore

$$\left.\begin{aligned}\tau_{13} &= -p_0 \\ \tau_{23} &= 0\end{aligned}\right\} \quad \text{for } r < \min(vt, r_c),$$
$$u_1 = u_2 = 0 \quad \text{for } r > \min(vt, r_c), \text{ and} \tag{11.37}$$
$$\tau_{33} = 0 \quad \text{for all } r$$

(p_0 is the stress drop, as discussed in more detail in Section 11.2).

The circular shape of the crack, which has a final radius of r_c, suggests cylindrical coordinates (r, ϕ, z) as the most convenient system to study the problem. We can rewrite the boundary conditions (11.37) as

$$\left.\begin{aligned}\tau_{rz} &= -p_0 \cos\phi \\ \tau_{\phi z} &= p_0 \sin\phi\end{aligned}\right\} \quad \text{for } r < \min(vt, r_c),$$
$$u_r = u_\phi = 0 \quad \text{for } r > \min(vt, r_c), \text{ and}$$
$$\tau_{zz} = 0 \quad \text{for all } r.$$

These boundary conditions have a simple sinusoidal azimuthal dependence. Consequently, we find that the ϕ-dependence of displacement components is either $\sin\phi$ or $\cos\phi$. They can be written as

$$u_r = u(r, z, t)\cos\phi, \quad u_\phi = v(r, z, t)\sin\phi, \quad u_z = w(r, z, t)\cos\phi.$$

The corresponding stress components can also be written in the same form:

$$\tau_{rr} = \Sigma_{rr}(r, z, t)\cos\phi, \quad \tau_{\phi\phi} = \Sigma_{\phi\phi}(r, z, t)\cos\phi, \quad \tau_{zz} = \Sigma_{zz}(r, z, t)\cos\phi,$$
$$\tau_{rz} = \Sigma_{rz}(r, z, t)\cos\phi, \quad \tau_{r\phi} = \Sigma_{r\phi}(r, z, t)\sin\phi, \quad \tau_{z\phi} = \Sigma_{z\phi}(r, z, t)\sin\phi.$$

Three components of particle velocity, $\dot{u}, \dot{v}, \dot{w}$, and six stress components make up nine unknowns, for which we have a system of nine first-order differential equations: three equations of motion and six equations from Hooke's law (the stress–strain relation). Denoting partial derivatives by a comma followed by the variable with respect to which the finite difference derivative is taken, the nine equations can be written as

$$\rho\dot{u}_{,t} = \frac{1}{r}(r\Sigma_{rr})_{,r} + \frac{1}{r}(\Sigma_{r\phi} - \Sigma_{\phi\phi}) + \Sigma_{rz,z},$$
$$\rho\dot{v}_{,t} = \frac{1}{r}(r\Sigma_{r\phi})_{,r} + \frac{1}{r}(\Sigma_{r\phi} - \Sigma_{\phi\phi}) + \Sigma_{z\phi,z},$$
$$\rho\dot{w}_{,t} = \frac{1}{r}(r\Sigma_{rz})_{,r} + \frac{1}{r}\Sigma_{z\phi} + \Sigma_{zz,z},$$
$$\Sigma_{rr,t} = (\lambda + 2\mu)\dot{u}_{,r} + \lambda(\dot{u} + \dot{v})/r + \lambda\dot{w}_{,z},$$
$$\Sigma_{zz,t} = \lambda\dot{u}_{,r} + \lambda(\dot{u} + \dot{v})/r + (\lambda + 2\mu)\dot{w}_{,z},$$
$$\Sigma_{\phi\phi,t} = \lambda\dot{u}_{,r} + (\lambda + 2\mu)(\dot{u} + \dot{v})/r + \lambda\dot{w}_{,z},$$
$$\Sigma_{r\phi,t} = \mu\dot{v}_{,r} - \mu(\dot{u} + \dot{v})/r, \qquad \Sigma_{z\phi,t} = \mu\dot{v}_{,z} - \mu\dot{w}/r, \qquad \Sigma_{zr,t} = \mu\dot{w}_{,r} + \mu\dot{u}_{,z},$$

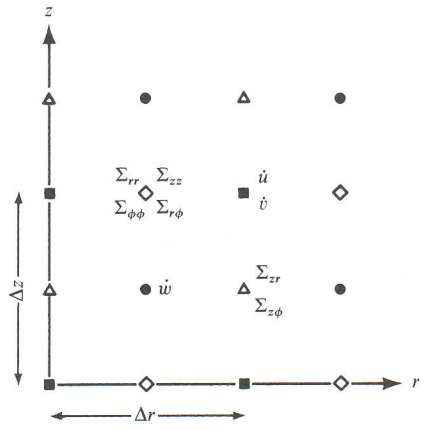

FIGURE **11.12**
Grid-point assignment for each of nine stress/particle-velocity components.

where λ, μ are the Lamé constants and ρ is the density. We have to solve these equations subject to the following boundary conditions on $z = 0$:

$$\Sigma_{rz} = -\Sigma_{\phi z} = -p_0 \qquad \text{for } r < \min(vt, r_c),$$

$$\dot{u} = \dot{v} = 0 \qquad \text{for } r < \min(vt, r_c), \text{ and}$$

$$\Sigma_{zz} = 0 \qquad \text{for all } r.$$

The slip components Δu_1 and Δu_2 in the original coordinates can be written in terms of u and v at $z = 0$:

$$\Delta u_1 = 2u \cos^2 \phi - 2v \sin^2 \phi, \qquad \Delta u_2 = (u + v) \sin 2\phi.$$

In the case of self-similar cracks studied in the preceding section, Δu_2 vanishes. In the present case Δu_2 does not necessarily vanish but is found to be practically negligible; i.e., $u \sim -v$, so that

$$\Delta u_1 = 2u = -2v. \tag{11.38}$$

Interestingly, Δu_1 is independent of ϕ.

Madariaga (1976) solved the above problem by the finite-difference method using a so-called staggered grid in which the velocities are defined at discrete times $k\,\Delta t$ and the stresses at times $(k + \frac{1}{2})\Delta t$, for integer values of k, where Δt is the time-grid interval. The spatial grid-point assignment for each of the nine stress-particle velocity components is shown in Figure 11.12.

Figure 11.13 shows the slip function $\Delta u(r, t) = u(r, +0, t) - u(r, -0, t)$ at several points on the crack. The rupture starts at $t = 0$ and expands with velocity 0.9β, where β is the shear velocity. The slip is measured with $p_0 r_c/\mu$ as the unit. The time t and radial distance r' are normalized to r_c/α and r_c, respectively, where α is the P-velocity. The slip function in time is shown at the center ($r = 0$) and at four other points at intervals of $0.2\,r_c$. At each position for which the slip history is shown, an arrow indicates the time of arrival of P-waves, originating from the perimeter of the crack at the instant the rupture

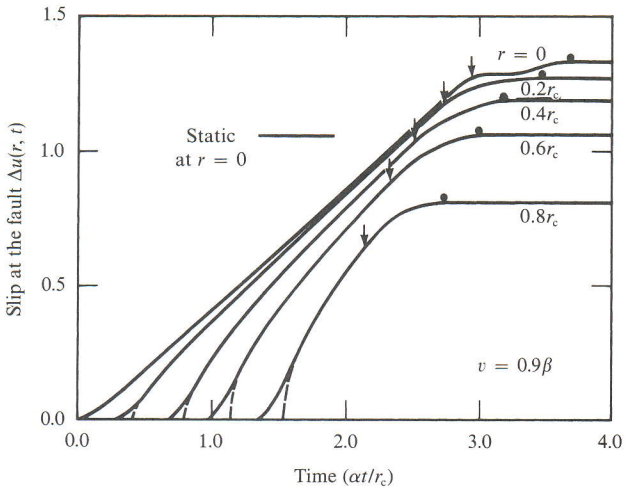

FIGURE **11.13**
Slip function at several distances from the center on the circular crack plotted against time. See text for explanation of symbols. [From Madariaga, 1976.]

stops. Figure 11.13 also shows the static slip expected at the center, $r = 0$. This level is low compared to the dynamic solutions for $r \leq 0.4\, r_c$, indicating a significant overshoot of dynamic slip. When the dynamic slip reaches a maximum and its velocity becomes zero, the slip is held fixed. (This would actually occur if static friction were large enough.) A closed circle indicates the time of slip arrest at each point. The broken curve at the initial rise shows the square-root function expected for the analytic solution. The numerical solution shows a less sharp rise because of the smoothing. This is an example of the effect of the artificially introduced end region discussed earlier.

The far-field displacement waveform corresponding to the slip function Δu_1 was given by equation (10.13), which in our present notation is

$$\Omega(\mathbf{x}, t) = \int_\Sigma \Delta \dot{u}_1 \left(\xi, t - \frac{R - (\xi \cdot \gamma)}{c} \right) d\Sigma,$$

where γ is the unit vector pointing to the receiver, ξ is the position vector of $d\Sigma$, and c is the speed of P- or S-waves. Writing the Fourier transform of $\Delta \dot{u}_1(\xi, t)$ as $\Delta \dot{u}_1(\xi, \omega)$, the far-field displacement spectrum can be obtained from equation (10.15) as

$$\Omega(\mathbf{x}, \omega) = e^{i\omega R/c} \int_\Sigma \Delta \dot{u}_1(\xi, \omega) \exp[-i\omega(\xi \cdot \gamma)/c]\, d\Sigma.$$

In our case, since $d\Sigma = r\, dr\, d\phi$ and Δu_1 is independent of ϕ, as shown in (11.38), we get

$$\Omega(\mathbf{x}, \omega) = e^{i\omega R/c} \int_0^{r_c} r\, dr\, \Delta \dot{u}_1(r, \omega) \int_{-\pi}^{\pi} \exp\left[i \frac{\omega r}{c} \sin\theta \cos(\phi - \phi_0) \right] d\phi,$$

where we have used $\xi \cdot \gamma = r \sin\theta \cos(\phi - \phi_0)$. Using the property of a Bessel function given prior to (6.7), we find

$$\Omega(\mathbf{x}, \omega) = 2\pi e^{i\omega R/c} \int_0^{r_c} r\, dr\, \Delta \dot{u}_1(r, \omega) J_0 \left(r \frac{\omega}{c} \sin\theta \right). \tag{11.39}$$

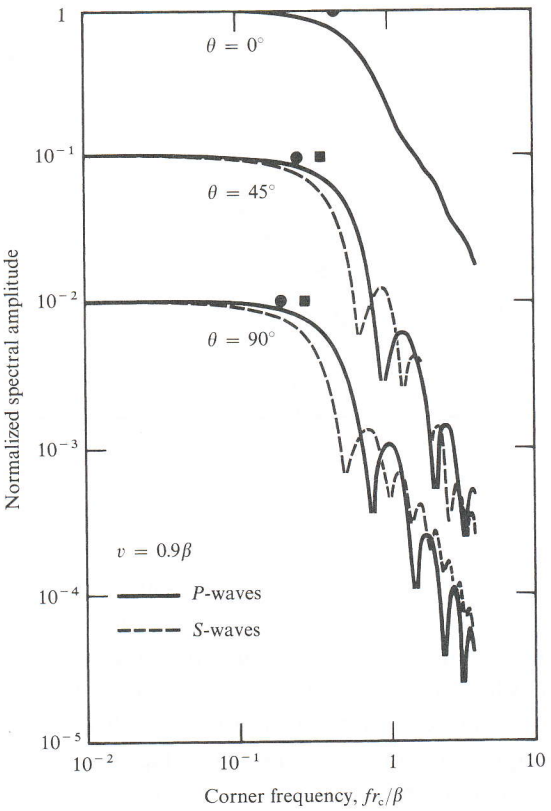

FIGURE **11.14**
Far-field spectra $|\Omega(\mathbf{x}, \omega)|$ for P- and S-waves in the case of rupture velocity $v = 0.9\beta$. [From Madariaga, 1976.]

This equation shows that the far-field displacement spectrum is a Hankel transform of $\Delta\dot{u}_1(r, \omega)$. As discussed for a more general case in Section 10.1.3, the far-field spectrum can recover the slip function only for wavenumbers less than ω/c, because $|\sin\theta| \leq 1$ for real θ.

The numerical solutions for $\Delta\dot{u}_1(r, t)$ are Fourier-transformed in t and Hankel-transformed in r to find the far-field spectrum $\Omega(\mathbf{x}, \omega)$ by (11.39). Figure 11.14 shows the resulting spectra, $|\Omega(\mathbf{x}, \omega)|$ for P- and S-waves at three receiver directions from a circular crack with rupture velocity $v = 0.9\beta$ ($\theta = 0$ corresponds to the normal to the crack plane). The spectra are flat at low frequencies and decay roughly as ω^{-2}. If the nucleation phase determines the high-frequency asymptote, we should have obtained ω^{-3}. We must, therefore, conclude that the stopping phase dominates the high-frequency spectrum, and the power of asymptotic decay is more like 2 (rather than like 3) in the case of a circular crack that suddenly stops.

The corner frequencies of the spectra were determined by the intersection of the low-frequency level and the high-frequency asymptote. They are indicated in Figure 11.14 by a closed circle for S-waves and a square for P-waves. The results for corner frequencies for various directions θ and rupture velocities are summarized in Figure 11.15. The corner frequencies are given in units of β/r_c for rupture velocities 0.6β, 0.7β, and 0.9β. Although the corner frequency increases with the rupture velocity, the variation is not very strong for

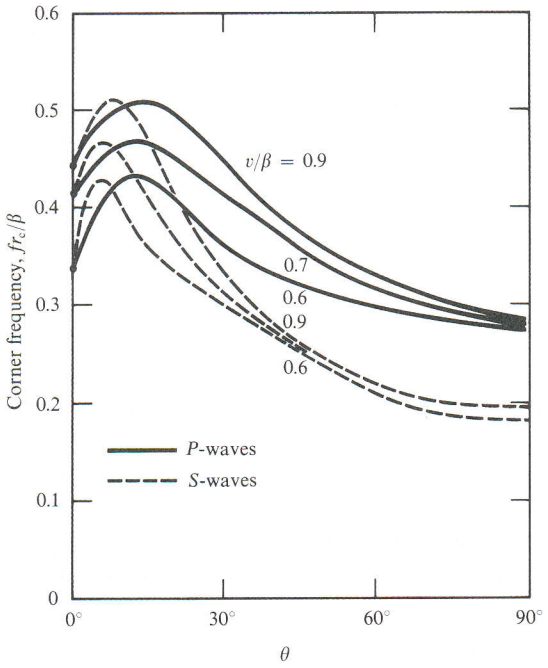

FIGURE **11.15**
Corner frequencies of P- and S-waves plotted against radiation direction for various rupture velocities. [From Madariaga, 1976.]

the range of rupture velocity considered here. The average values of the corner frequencies over all directions, for the case of $v = 0.9\beta$, are given by

$$f_c^P \text{ (in Hz)} = 0.32\beta/r_c \qquad f_c^S \text{ (in Hz)} = 0.21\beta/r_c$$

for P- and S-waves, respectively. The above equations predict considerably lower corner frequencies (by about a factor of 2) than Brune's (1970) formula, which was derived from a simple kinematic approach and which has been widely used in the interpretation of observed seismic spectra. The corner frequency for P-waves is higher than for S-waves, as expected from the earlier result of Molnar *et al.* (1973) for kinematic models with a similar slip function (see Figure 10.12 and Section 10.1.6).

11.2 Dynamics of Spontaneous Planar Rupture Propagation

One of the most challenging problems in seismology is to predict the occurrence of an earthquake and the resultant seismic motion from the study of physical properties of rocks in the epicentral region and the tectonic stress existing in the region. In order to approach this problem, we must go beyond the treatment of rupture propagation in the preceding section, in which the nucleation, propagation, and stopping of a rupture front are arbitrarily prescribed. There are three important lines of work to be carried out before we solve this problem. First, we must study properties of fault-gouge material, such as the specific surface energy, the length of the end region, and the static and dynamic values of friction and their distribution in space. Second, we must determine the tectonic stress acting on the fault

zone. Third, we must be able to predict the entire rupture phenomena from beginning to end solely on the basis of the initial stress condition and material properties of the fault zone. In this section, we shall consider the last aspect of the problem for an idealized case. We shall concentrate on how the stress distribution and the fracture criterion determine the movement of a crack tip, and (consequently) the slip function. For simplicity we shall confine our attention to planar shear cracks in an infinite homogeneous medium (so that the normal stress is unchanged by the rupture process—see Problem 10.2). We start with the case of an anti-plane crack, following the pioneering work of Kostrov (1966).

11.2.1 SPONTANEOUS PROPAGATION OF AN ANTI-PLANE CRACK: GENERAL THEORY

Using the (x, y, z) coordinates shown in Figure 10.19, we define the crack as

$$x_1 < x < x_2, \quad -\infty < z < \infty, \quad \text{and } y = 0.$$

For an anti-plane case (Section 10.2.3), only the z-component of displacement $w(x, y, t)$ is nonzero, and the only nonvanishing elements of the stress tensor are $\tau_{zx} = \mu(\partial w/\partial x)$ and $\tau_{yx} = \mu(\partial w/\partial y)$. The problem is two-dimensional, with no dependence on z. The equation of motion in this case reduces to the wave equation

$$\frac{1}{\beta^2}\frac{\partial^2 w}{\partial t^2} = \frac{\partial^2 w}{\partial x^2} + \frac{\partial^2 w}{\partial y^2}, \tag{11.40}$$

where $\beta = \sqrt{\mu/\rho}$ is the shear velocity.

Suppose that initially the crack is absent and the body is in equilibrium with an initial state of stress $\boldsymbol{\sigma}^0$. We shall take this initial state as the reference state and measure the displacement relative to this state. The total stress is then $\boldsymbol{\sigma} = \boldsymbol{\sigma}^0 + \boldsymbol{\tau}$, where the incremental stress $\boldsymbol{\tau}$ is derived from $\mathbf{u}$ by Hooke's law. Initial conditions are that w and $\partial w/\partial t$ are zero for $t = 0$. When the crack is formed (i.e., when a displacement discontinuity develops across the crack), the traction on the crack drops to the dynamic frictional stress. The only changing component of traction on the crack ($y = 0$) is σ_{yz}, and it changes from its original value σ^0_{yz} to a new value, say σ^{d}_{yz}. We shall equate the stress drop $\sigma^0_{yz}(x, 0) - \sigma^{\mathrm{d}}_{yz}(x, 0, t)$ to $p(x, t)$. The appropriate boundary condition for traction on the crack for the above choice of reference state is then given by

$$\tau_{yz} = -p(x, t) \qquad \text{for } x_1 < x < x_2, \quad y = 0. \tag{11.41}$$

In order to find the boundary condition outside of (x_1, x_2) on $y = 0$, we first need to establish that $w(x, y, t)$ is an odd function of y. This is done by writing the solution of equation (11.40) as

$$w = \iint \acute{w}(\omega, k) \exp(-i\omega t + ikx - \nu y)\, d\omega\, dk \qquad y > 0$$

$$= \iint \grave{w}(\omega, k) \exp(-i\omega t + ikx + \nu y)\, d\omega\, dk \qquad y < 0,$$

where $\nu = \sqrt{k^2 - \omega^2/\beta^2}$ and $\operatorname{Re}\nu \geq 0$ because of the radiation condition. Continuity of traction τ_{yz} across $y = 0$ then gives

$$\acute{w}(\omega, k) = -\grave{w}(\omega, k),$$

so $w(x, y, t)$ must indeed be an odd function of y. Secondly we note that an odd function of y must be zero at $y = 0$ if it is continuous there. Since w is continuous at $y = 0$ outside the crack, it follows that

$$w(x, y, t) = 0 \qquad x < x_1, x_2 < x, y = 0. \tag{11.42}$$

Equations (11.41) and (11.42) together give what is called a mixed boundary condition on $y = 0$. Because of the symmetry, it is sufficient to obtain a solution only in the half-space $y < 0$.

To solve this boundary-value problem, let us start with the representation theorem (2.43), using the Green function that satisfies the stress-free condition on the surface $y = 0$. Since displacements and stresses are independent of z, the relevant form of (2.43) is

$$w(x_0, y_0, t_0) = \int_{-\infty}^{\infty} dt \int_{-\infty}^{\infty} G_{33}^{\text{free}}(x_0, y_0, t_0; x, 0, t)\, T_3(x, 0, t)\, dx \tag{11.43}$$

where G_{33} is the displacement at (x_0, y_0, t_0) in the direction perpendicular to (x_0, y_0) for a line source at $(x, 0, t)$ in the direction perpendicular to (x, y).

Such a Green function, entailing only SH-waves, can be obtained by first finding the Green function G for a full space corresponding to a line body-force impulse located at $(x, 0, t)$:

$$\rho \frac{\partial^2 G}{\partial t_0^2} - \mu \frac{\partial^2 G}{\partial x_0^2} - \mu \frac{\partial^2 G}{\partial y_0^2} = \delta(x_0 - x)\, \delta(y_0)\, \delta(t_0 - t).$$

Apart from differences in notation, this is the equation (6.42) that is solved by (6.43), and for our present purposes we obtain the full space solution as

$$G(x_0, y_0, t_0; x, 0, t) = \frac{H\left[(t_0 - t) - \sqrt{(x_0 - x)^2 + y_0^2}/\beta\right]}{2\pi\mu R},$$

where $R^2 = (t_0 - t)^2 - [(x_0 - x)^2 + y_0^2]/\beta^2$ and $H[\ ]$ is the unit step function. Since the full-space Green function G, with a source on $y = 0$, satisfies the stress-free condition at $y_0 = 0$, the Green function G_{33}^{free} for a source on the free surface $y_0 = 0$ is merely $2G$, where the effect of reflection is taken care of by doubling the amplitude. That is,

$$G_{33}^{\text{free}}(x_0, y_0, t_0; x, 0, t) = 2G(x_0, y_0, t_0; x, 0, t). \tag{11.44}$$

Another way to obtain (11.44) is to use reciprocity and the result given in Problem 5.6 for SH-waves recorded on a free surface.

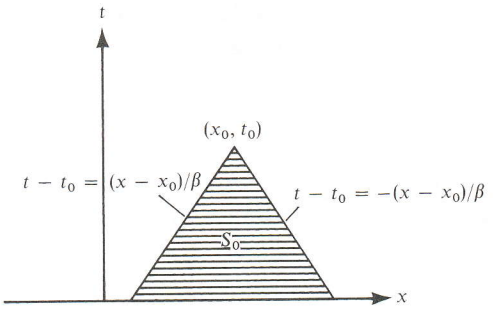

FIGURE **11.16**
All points within S_0 can influence the displacement at (x_0, t_0).

In terms of the traction $T_3 = \tau_{yz} = \tau(x, t)$, say, for all x on $y = 0$, we can write the solution for displacement w by putting $2G(x_0, t_0; x, t)$ into the representation (11.43) as

$$w(x_0, y_0, t_0) = \frac{1}{\pi\mu} \iint_S \frac{\tau(x,t)}{R}\, dx\, dt \qquad y_0 < 0, \tag{11.45}$$

where S is that part of the xt-plane which lies inside the cone

$$\beta^2(t_0 - t)^2 - (x_0 - x)^2 - y_0^2 \geq 0 \qquad 0 \leq t \leq t_0.$$

For $y_0 = 0^-$, we obtain

$$w(x_0, 0^-, t_0) = \frac{1}{\pi\mu} \iint_{S_0} \frac{\tau(x,t)\, dx\, dt}{\sqrt{(t_0 - t)^2 - (x_0 - x)^2/\beta^2}}, \tag{11.46}$$

where S_0, shown as the shaded area in Figure 11.16, is the triangle

$$\beta^2(t_0 - t)^2 - (x_0 - x)^2 \geq 0 \qquad 0 \leq t \leq t_0.$$

Since we do not yet know $\tau(x, t)$ for the whole area of S_0, equation (11.46) does not immediately give the solution. To find τ we can use (11.42), to obtain the following equation for $x_0 < x_1$ and $x_0 > x_2$:

$$\iint_{S_0} \frac{\tau(x,t)\, dx\, dt}{\sqrt{(t_0 - t)^2 - (x_0 - x)^2/\beta^2}} = 0.$$

$\tau(x, t)$ is known in some parts of the above integration region S_0, shown in Figure 11.17, where the loci of crack tips are indicated by $x_1(t)$ and $x_2(t)$. The subregion S_1 lies inside the crack, and $\tau(x, t)$ is known there from (11.41). We also know that $\tau(x, t)$ is zero in the subregion $S_0 - S_1 - S_2$, for which $x > x_2(0) + \beta t$, because any disturbances from the crack have not yet reached this subregion. The value of $\tau(x, t)$ in subregion S_2 is unknown.

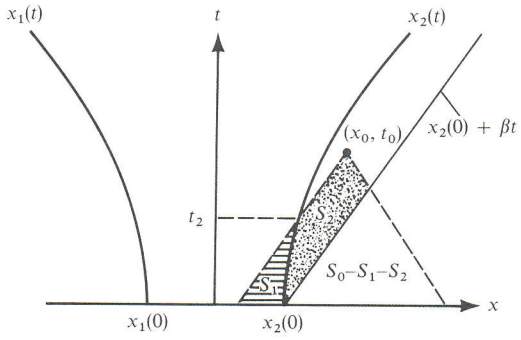

FIGURE **11.17**
$\tau(x,t)$ is known in S_1, but unknown in S_2. It is zero in $S_0 - S_1 - S_2$.

Thus, as long as S_0 does not intersect $x_1(t)$ (when the disturbances from the left crack tip have not yet reached the observation point), for $x_0 < x_1$ and $x_0 > x_2$ we have

$$\iint_{S_2} \frac{\tau(x,t)\,dx\,dt}{\sqrt{(t_0-t)^2-(x_0-x)^2/\beta^2}} = \iint_{S_1} \frac{p(x,t)\,dx\,dt}{\sqrt{(t_0-t)^2-(x_0-x)^2/\beta^2}}. \quad (11.47)$$

To solve this integral equation for $\tau(x,t)$ in S_2, we make the following transformation:

$$\xi = (\beta t - x)/\sqrt{2}, \qquad \eta = (\beta t + x)/\sqrt{2}. \quad (11.48)$$

Then (11.47) can be rewritten as

$$\int_{-x_2(0)/\sqrt{2}}^{\xi_0} \frac{d\xi}{\sqrt{\xi_0-\xi}} \int_{\eta_2(\xi)}^{\eta_0} \frac{\tau(\xi,\eta)\,d\eta}{\sqrt{\eta_0-\eta}} = \int_{-x_2(0)/\sqrt{2}}^{\xi_0} \frac{d\xi}{\sqrt{\xi_0-\xi}} \int_{-\xi}^{\eta_2(\xi)} \frac{p(\xi,\eta)\,d\eta}{\sqrt{\eta_0-\eta}} \quad (11.49)$$

where $\eta_2(\xi)$ is the solution of

$$\eta_2 - \xi = \sqrt{2}x_2\left(\frac{\eta_2+\xi}{\sqrt{2}\beta}\right),$$

which defines the position of the right crack tip in terms of ξ and η. The integration limits for ξ and η can be found from Figure 11.18, and (11.49) will be satisfied if

$$\int_{\eta_2(\xi)}^{\eta_0} \frac{\tau(\xi,\eta)\,d\eta}{\sqrt{\eta_0-\eta}} = \int_{-\xi}^{\eta_2(\xi)} p(\xi,\eta)\frac{d\eta}{\sqrt{\eta_0-\eta}}. \quad (11.50)$$

Equation (11.50) is in the form of Abel's integral equation for $\tau(\xi,\eta)$. The solution is described in Box 9.3, and in our case we find

$$\tau(\xi_0,\eta_0) = \frac{1}{\pi}\frac{d}{d\eta_0}\int_{\eta_2(\xi_0)}^{\eta_0} \frac{d\eta_1}{\sqrt{\eta_0-\eta_1}} \int_{-\xi_0}^{\eta_2(\xi_0)} p(\xi_0,\eta)\frac{d\eta}{\sqrt{\eta_1-\eta}}.$$

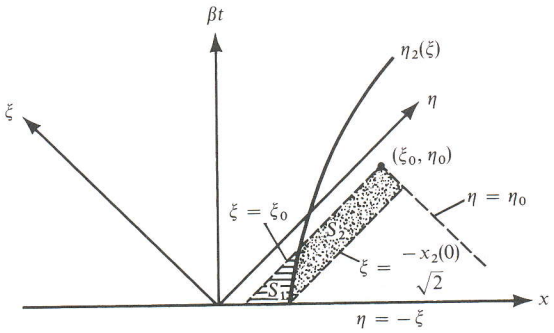

FIGURE **11.18**
Change of integral variables from (x, t) to (ξ, η).

Since

$$\int_{\eta_2}^{\eta_0} \frac{d\eta_1}{\sqrt{\eta_0 - \eta_1}\sqrt{\eta_1 - \eta}} = \sin^{-1}\left(1 + \frac{2(\eta_0 - \eta_1)}{\eta - \eta_0}\right)\Bigg|_{\eta_1=\eta_2}^{\eta_1=\eta_0},$$

the above equation reduces to

$$\tau(\xi_0, \eta_0) = \frac{1}{\pi\sqrt{\eta_0 - \eta_2(\xi_0)}} \int_{-\xi_0}^{\eta_2(\xi_0)} p(\xi_0, \eta) \frac{\sqrt{\eta_2(\xi_0) - \eta}}{\eta_0 - \eta}\, d\eta. \tag{11.51}$$

The path of integration is along $\xi = \xi_0$, which corresponds to the path $t - t_0 = (x - x_0)/\beta$ in xt-coordinates. Transforming back to xt-coordinates, and referring to Figures 11.17 and 11.18, we obtain

$$\tau(x_0, t_0) = \frac{1}{\pi\sqrt{x_0 - x_2(t_2)}} \int_{x_0 - \beta t_0}^{x_2(t_2)} p[x, t_0 + (x - x_0)/\beta] \frac{\sqrt{x_2(t_2) - x}}{x_0 - x}\, dx \tag{11.52}$$

for $x_0 > x_2(t_0)$, where t_2 is the solution of

$$\beta t_0 - x_0 = \beta t_2 - x_2(t_2).$$

In other words, t_2 is the time at which the crack-tip locus $x_2(t)$ intersects the integration path. The above expression is valid for the time interval $0 < t_0 < [x_0 - x_1(0)]/\beta$. A similar result may be obtained for the region $x_0 < x_1$ for the time interval $0 < t_0 < [x_2(0) - x_0]/\beta$. To determine $\tau(x_0, t_0)$ for later periods, additional subregions of S_0 with unknown $\tau(x, t)$ appear, corresponding to repeated diffraction of the waves at the crack boundary.

Equation (11.52) shows that the stress $\tau(x_0, t_0)$ becomes infinite when the crack tip arrives at the receiver, so that $x_0 = x_2(t_0)$. At any given time t_0 prior to arrival, the distance between the crack tip and the receiver is $x_0 - x_2(t_0)$. Using the stress-intensity factor K defined in Section 11.1.1, $\tau(x_0, t_0)$ near and ahead of the crack tip can be written as

$$\tau(x_0, t_0) \sim \frac{K}{\sqrt{2\pi[x_0 - x_2(t_0)]}}. \tag{11.53}$$

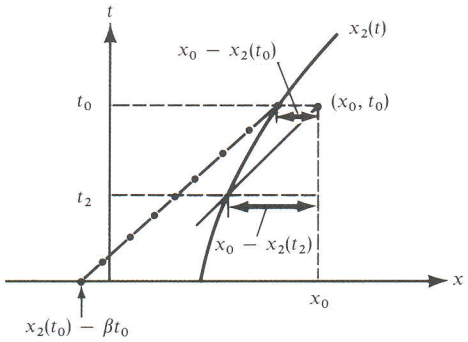

FIGURE **11.19**
Integration path for (11.55).

On the other hand, as can be seen from Figure 11.19,

$$x_0 - x_2(t_2) = \beta(t_0 - t_2),$$
$$x_2(t_0) - x_2(t_2) \sim \dot{x}_2(t_0)(t_0 - t_2),$$

and therefore

$$\frac{x_0 - x_2(t_0)}{x_0 - x_2(t_2)} \sim 1 - \dot{x}_2(t_0)/\beta. \tag{11.54}$$

Comparing (11.52), (11.53), and (11.54), we find that

$$K = \frac{\sqrt{1 - \dot{x}_2(t_0)/\beta}}{\sqrt{\pi/2}} \int_{x_2(t_0)-\beta t_0}^{x_2(t_0)} p\{x, t_0 - [x_2(t_0) - x]/\beta\} \frac{dx}{\sqrt{x_2(t_0) - x}} \tag{11.55}$$

near the crack tip, where $x_0 \sim x_2(t_2) \sim x_2(t_0)$. The integration path is a straight line, shown connecting $[t_0, x_2(t_0)]$ and $[0, x_2(t_0) - \beta t_0]$ in Figure 11.19.

In Section 11.1.2, we showed that the tip of an anti-plane crack moving with a subsonic velocity v absorbs energy at a rate given by

$$g = \frac{vK^2}{2\mu} \Big/ \sqrt{1 - \frac{v^2}{\beta^2}}. \tag{11.15 again}$$

Expressing the surface energy required to create a new unit area as G, we have

$$G = \frac{g}{2v} = \frac{K^2}{4\mu} \Big/ \sqrt{1 - \frac{v^2}{\beta^2}}.$$

Combining this equation with (11.55) (and dropping the subscript 0 from t_0), we obtain

$$K = 2\sqrt{\mu G}(1 - v^2/\beta^2)^{1/4}$$
$$= \sqrt{\frac{2}{\pi}} \sqrt{1 - v/\beta} \int_{x_2-\beta t}^{x_2} p[x, t - (x_2 - x)/\beta] \frac{dx}{\sqrt{x_2 - x}}$$

or

$$\int_{x_2-\beta t}^{x_2} p[x, t-(x_2-x)/\beta]\frac{dx}{\sqrt{x_2-x}} = \sqrt{2\mu\pi G}\left(\frac{1+v/\beta}{1-v/\beta}\right)^{1/4}, \qquad (11.56)$$

where $v = \dot{x}_2(t)$. This equation, first derived by Kostrov (1966), gives the velocity of the crack tip for given $p(x,t)$ and G. Equation (11.56) holds only when

$$\int_{x_2-\beta t}^{x_2} p[x, t-(x_2-x)/\beta]\frac{dx}{\sqrt{x_2-x}} \geq \sqrt{2\mu\pi G}.$$

Otherwise, the crack tip does not move.

Once the locus $x_2(t)$ of the crack tip is determined, $\tau(x_0, t_0)$ can be calculated by equation (11.51). Then we can use (11.45) to determine the displacement at any point. In fact, the displacement inside the crack can be determined using only the stress drop $p(x,t)$ inside the crack. To see this, we transform the variables (x,t) to (ξ,η) by equation (11.48), and rewrite (11.46) as

$$w(\xi_0,\eta_0) = \frac{1}{\pi\mu}\iint \frac{\tau(\xi,\eta)\,d\xi\,d\eta}{\sqrt{2}\sqrt{\xi_0-\xi}\sqrt{\eta_0-\eta}} \qquad \text{on } y = 0^-.$$

Next, we divide the area of integration into four parts, as shown in Figure 11.20. In S_1 and S_3, $-\tau(\xi,\eta)$ is given as the stress drop $p(\xi,\eta)$. In S_2, $\tau(\xi,\eta)$ is unknown but is determined by equation (11.51) using $p(\xi,\eta)$. In the remaining parts of S_0, $\tau(\xi,\eta)$ vanishes.

From equation (11.50), for a point (ξ_1,η_1) close to the crack-tip locus but outside the crack, we have

$$\int_{\eta_2(\xi)}^{\eta_1} \frac{\tau(\xi_1,\eta)\,d\eta}{\sqrt{\eta_1-\eta}} - \int_{-\xi_1}^{\eta_2(\xi)} \frac{p(\xi_1,\eta)\,d\eta}{\sqrt{\eta_1-\eta}} = 0.$$

Our integral with respect to η for the areas S_1 and S_2 is exactly of the above form, with $\eta_0 = \eta_1$. Thus the contributions from S_1 and S_2 are zero. The only contribution comes from S_3, so that the displacement on $y = 0^-$ is

$$w(\xi_0,\eta_0) = \frac{-1}{\sqrt{2}\pi\mu}\int_{\xi_2(\eta_0)}^{\xi_0}\frac{d\xi}{\sqrt{\xi_0-\xi}}\int_{-\xi}^{\eta_0}\frac{p(\xi,\eta)\,d\eta}{\sqrt{\eta_0-\eta}}, \qquad (11.57)$$

where $\xi = \xi_2(\eta)$ is the locus of the crack tip in the (ξ,η) plane. The above equation, giving the fault slip $(2w)$ as a function of stress drop $p(\xi,\eta)$ and crack-tip location $\xi_2(\eta)$, was used by Ida (1973) in a study of spontaneous rupture propagation that is one of the examples we take up in the next section.

11.2.2 EXAMPLES OF SPONTANEOUS ANTI-PLANE CRACK PROPAGATION

Let us find how the equation of crack tip motion, (11.56), is solved for some simple examples.

BOX **11.3**

The stress-intensity factor associated with cohesive force alone

Here we shall show that equation (11.55) can be used to derive (11.19) for the case of a crack tip moving at constant velocity.

Let the coordinate in the x-direction in a frame moving with the crack tip at a velocity v be x'. Then $x' = x - x_2(t)$, where $x_2(t) = \text{constant} + vt$.

We have previously defined p as the stress drop $\sigma^0_{yz} - \sigma^d_{yz}$. But if a cohesive force is considered, as in (11.18), the stress on the fault plane becomes $\sigma^d_{yz} + \sigma_c$, so that the stress drop is $\sigma^0_{yz} - \sigma^d_{yz} - \sigma_c$, i.e., it is augmented by an amount $-\sigma_c$. The effect of the cohesive force is therefore to add a stress concentration, with the stress-intensity factor derived from (11.55) by replacing p with $-\sigma_c$. The integration is limited to the region $-d \le x' \le 0$ in which $\sigma_c \neq 0$, and all this range is included in the integration limits of (11.55).

As can easily be seen from the figure,

$$x_2(t_0) - x = \frac{\beta}{\beta - v}(-x') \qquad \text{and} \qquad dx = \frac{\beta}{\beta - v}\,dx'.$$

Therefore, equation (11.55) is transformed to

$$K = -\sqrt{\frac{2}{\pi}} \int_{-d}^{0} \sigma_c(x') \frac{dx'}{\sqrt{-x'}},$$

which is the result used earlier in (11.19). Note that K is independent of v in this case.

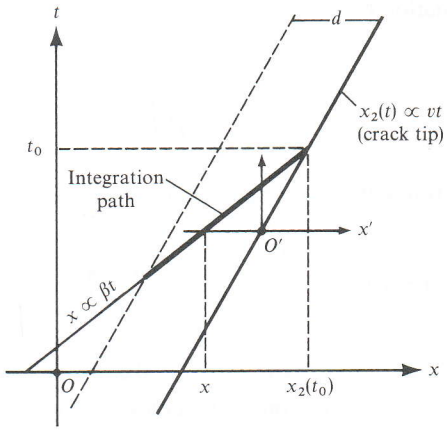

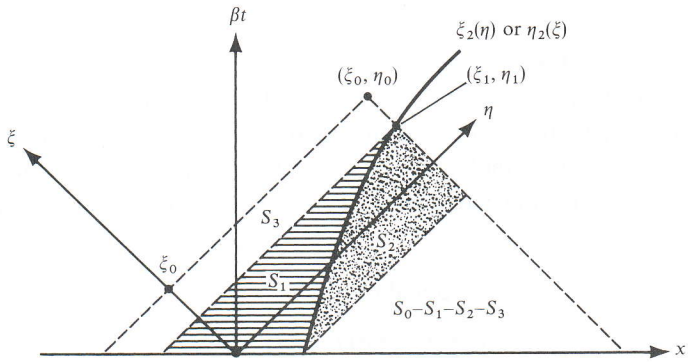

FIGURE **11.20**

A SEMI-INFINITE CRACK

Consider an unbounded body under a uniform shear stress σ_{yz}^0. A crack appears instantaneously at $t = 0$ over the half-plane $y = 0, x < 0$. Assuming that the dynamic friction is zero, a stress drop of σ_{yz}^0 occurs instantaneously for $y = 0, x < 0$. We shall find the position $x_2(t)$ of the crack tip $t > 0$ using the equation of crack-tip motion. Since

$$p(x,t) = \sigma_{yz}^0 \qquad \text{for } x < x_2(t),$$

we have from equation (11.56)

$$\int_{x_2-\beta t}^{x_2} \frac{\sigma_{yz}^0\, dx}{\sqrt{x_2 - x}} = \sqrt{2\mu\pi G}\left(\frac{1+\dot{x}_2/\beta}{1-\dot{x}_2/\beta}\right)^{1/4}. \tag{11.58}$$

The left-hand side here is equal to $2\sigma_{yz}^0\sqrt{\beta t}$. The above equation cannot be satisfied for t smaller than t_c given by

$$2\sigma_{yz}^0\sqrt{\beta t_c} = \sqrt{2\mu\pi G}, \tag{11.59}$$

and the crack tip does not propagate until time t_c. Once this time is passed, the crack-tip motion is governed by equation (11.58), i.e.,

$$\sqrt{\frac{t}{t_c}} = \left(\frac{1+\dot{x}_2/\beta}{1-\dot{x}_2/\beta}\right)^{1/4}.$$

Solving for $\dot{x}_2$ and integrating with respect to t from t_c to t, we find

$$x_2(t) = \beta t - \beta t_c\left[1 + 2\tan^{-1}\left(\frac{t}{t_c}\right) - \frac{\pi}{2}\right].$$

The crack tip starts moving at $t = t_c$ with zero initial velocity, rapidly reaching a terminal velocity β. Figure 11.21 shows the motion of the crack tip for different t_c. The solid lines correspond to the Irwin criterion in which the critical stress-intensity factor is assumed to be a material constant, independent of rupture velocity (see Problem 11.3). The step-like curves are obtained by a numerical method that is discussed later.

A SEMI-INFINITE CRACK THAT STOPS

The above classic example given by Kostrov (1966) was extended by Husseini *et al.* (1975) to include the stopping of crack-tip motion. The crack-tip motion can be stopped by placing a barrier of high surface energy along the fault plane or by limiting the prestressed region to a finite size. In either case, the following condition is imposed on the stress drop $p(x,t)$ over the initial semi-infinite crack:

$$\begin{aligned} p(x,t) &= 0 \qquad && \text{for } x < -a \text{ and } t > 0, \\ &= p_0 \qquad && \text{for } -a < x < x_2(t) \text{ and } t > 0, \end{aligned}$$

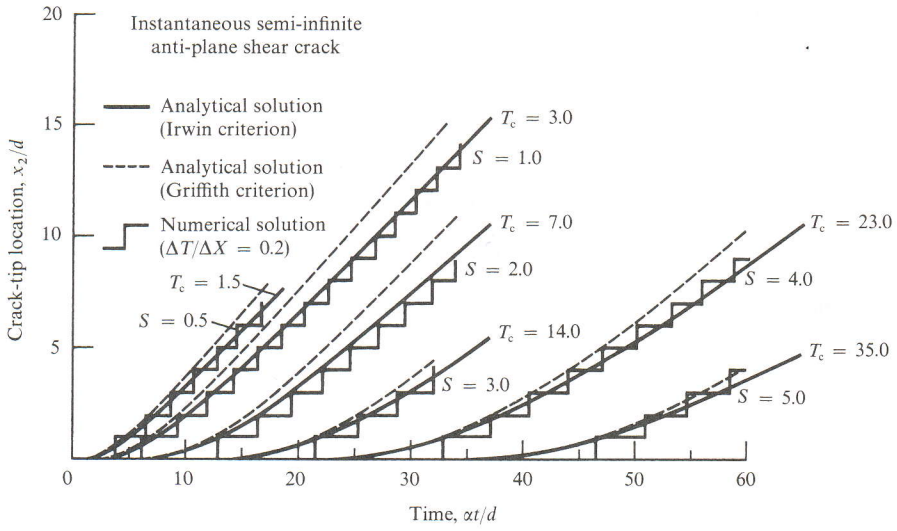

FIGURE **11.21**
The crack-tip location x_2 as a function of time for various values of T_c, where $T_c = \alpha t_c/d$, α is the compressional wave velocity, t_c is the rupture starting time defined in (11.59), and d is the grid length used in the numerical solution described in Section 11.2.3. S is the parameter of a fracture criterion used in the numerical solution, and $1 + S = S_c/(\sigma^0_{xy} - \sigma^d_{xy})$, where S_c is the critical stress difference defined in (11.78). Broken curves correspond to the criterion of constant surface energy, and solid curves to the criterion of constant critical stress-intensity factor. [From Das and Aki, 1977a.]

where p_0 is a constant. This is intended to simulate a finite crack without introducing complex multiple diffractions at crack edges. For a given p_0 and specific surface energy G_0 at $x = 0$, a must be greater than βt_c so that the rupture can be initiated. From (11.59), the condition is

$$a > \frac{\mu\pi G_0}{2p_0^2}.$$

The rupture can be stopped by making G increase with x. For example, consider a linearly increasing surface energy

$$G(x) = (1 + mx)G_0.$$

From equation (11.56), we get

$$\begin{aligned} \dot{x}_2(t) &= \beta \frac{t^2 - t_c^2(1 + mx_2)^2}{t^2 + t_c^2(1 + mx_2)^2} && x_2 - \beta t > -a \\ &= \beta \frac{(x_2 + a)^2/\beta^2 - t_c^2(1 + mx_2)^2}{(x_2 + a)^2/\beta^2 + t_c^2(1 + mx_2)^2} && x_2 - \beta t < -a. \end{aligned} \tag{11.60}$$

The stopping position of the crack tip, x_s, may be obtained from the second equation in (11.60) by setting $\dot{x}_2(t) = 0$. Then

$$x_s = \frac{a - \beta t_c}{m\beta t_c - 1}.$$

Since the solution x_s must be positive, the rate m of increase in specific energy must be greater than $(\beta t_c)^{-1}$ for the crack tip to stop. The motion of the crack tip can be obtained by solving the differential equation (11.60).

Another simple case of a barrier is a step-like increase in G:

$$\begin{aligned} G &= G_0 \qquad & 0 \le x < b, \\ G &= G_0 + \Delta G \qquad & b < x. \end{aligned}$$

In this case, for $x_2(t) > b$, we have

$$\dot{x}_2 = \frac{(x_2 + a)^2/\beta^2 - t_c^2[1 + (\Delta G/G_0)]^2}{(x_2 + a)^2/\beta^2 + t_c^2[1 + (\Delta G/G_0)]^2}, \tag{11.61}$$

and setting $\dot{x}_2 = 0$ we can solve for the stopping position of the tip,

$$x_s = \beta t_c[1 + (\Delta G/G_0)] - a.$$

Since $x_s \ge b$, an inequality has to be satisfied for the stopping to occur:

$$\beta t_c \left(1 + \frac{\Delta G}{G_0}\right) = \frac{\mu\pi(G_0 + \Delta G)}{2p_0^2} \ge (a + b). \tag{11.62}$$

If we put this condition into equation (11.61), we find $\dot{x}_2$ to be zero or negative. Since $\dot{x}_2$ cannot be negative physically, $\dot{x}_2$ must vanish and the equality holds in (11.62). The equality means that $x_s = b$, or that the crack tip stops immediately at b if condition (11.62) holds. If not, the tip will propagate indefinitely beyond b. For example, if $G_0 = 10^4$ erg/cm^2, $(a + b) = 1$ km, $p_0 = 10$ bar, and $\mu = 3 \times 10^{11}$ dyn/cm^2, then ΔG must be about 10^7 erg/cm^2 or greater for the rupture to stop. Furthermore, the larger the length or the larger the stress drop, the greater ΔG must be to stop the rupture.

An alternative way of stopping a rupture is to limit the size of the prestressed region. For example, consider the case in which, for $t > 0$,

$$\begin{aligned} p(x,t) &= 0 \qquad & \text{for } x < -a \\ &= p_0 \qquad & -a < x < x_2(t) < b \\ &= 0 \qquad & b < x. \end{aligned}$$

The equation of motion (11.56) gives the crack-tip velocity as

$$\dot{x}_2 = \frac{[f(x_2,t)]^4 - \beta^2 t_c^2}{[f(x_2,t)]^4 + \beta^2 t_c^2},$$

where

$$\begin{aligned} f(x_2,t) &= \sqrt{\beta t} && x_2 < b,\ x_2 - \beta t > -a \\ &= \sqrt{x_2 + a} && x_2 - \beta t < -a \\ &= \sqrt{\beta t} - \sqrt{x_2 - b} && x_2 > b,\ x_2 - \beta t > -a \\ &= \sqrt{x_2 + a} - \sqrt{x_2 - b} && x_2 - \beta t < -a. \end{aligned}$$

From the final equation, the stopping position may be obtained by setting $\dot{x}_2 = 0$. Then

$$x_s = \frac{(a+b)^2}{4\beta t_c} + \frac{b-a}{2} + \frac{\beta t_c}{4}.$$

For example, if $b \sim a \sim \beta t_c$, then $x_s \sim b(1 + \frac{1}{4})$; but if $b \gg a \sim \beta t_c$, then $x_s \sim b(1 + b/4a)$. Thus, if the length b of the prestressed region is much greater than $\beta t_c = \mu\pi G_0/2p_0^2$, there will be a considerable overshoot of crack extension into the initially unstressed region. For typical values of the surface energy G measured in the laboratory ($\sim 10^4$ ergs/cm^2), and $\tau_0 = 10$ bar, βt_c is only 50 cm. However, as mentioned in Section 11.1.3, the real value of G for earthquakes may be around 10^8 erg/cm^2, which corresponds to values of βt_c around 5 km. Since G is expected to increase with earthquake magnitude because of increase in the zone of microcrack formation and plastic deformation, overshoot may not play a very important role in practice.

Slip-rate-dependent boundary condition on the fault

If there should be any constitutive relation between the stress and slip, or between stress and slip rate, it can be incorporated into our equation of rupture propagation. For example, Ida (1973) assumed that the stress σ_{yz} on the fault is related to the slip rate $\Delta\dot{w}$ by the following equation (see Fig. 11.22):

$$\begin{aligned} \sigma_{yz} &= \gamma\, \Delta\dot{w} && \text{for } \Delta\dot{w} \le v_c \\ &= \sigma_{yz}^{d} && \text{for } \Delta\dot{w} > v_c, \end{aligned} \tag{11.63}$$

where σ_{yz} is *total* stress acting on the fault plane, i.e., the sum of the initial stress σ_{yz}^0 and the stress increment τ_{yz} due to crack formation. The slip rate $\Delta\dot{w}$ is equal to $-2\dot{w}$ for $\dot{w}$ evaluated on $y = 0^-$ (which is the side of the fault for which we have studied displacement; see, e.g., (11.45)). Although the above constitutive relation is not very realistic, it does display a transition from ductile to brittle behavior. This may grossly simulate the behavior of an earthquake fault on which creep and dynamic failure are both occurring.

Suppose we start with an initially unstressed fault. As the tectonic stress increases, slow creep may occur across the fault, and the slip rate may increase in proportion to the stress. When the slip rate reaches a certain yield limit v_c, the stress may suddenly drop to the dynamic friction level σ_{yz}^{d}, creating an earthquake.

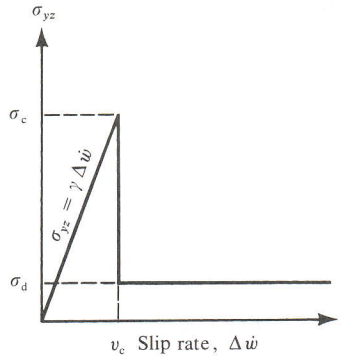

FIGURE **11.22**
Constitutive relation between the stress across the fault plane and slip rate given by (11.63). [From Ida, 1973; copyright by the American Geophysical Union.]

To incorporate the above constitutive relation into the equation of rupture propagation, we make use of

$$w(\xi_0, \eta_0) = \frac{-1}{\sqrt{2}\pi\mu} \int_{\xi_2(\eta_0)}^{\xi_0} \frac{d\xi}{\sqrt{\xi_0 - \xi}} \int_{-\xi}^{\eta_0} \frac{p(\xi, \eta)\, d\eta}{\sqrt{\eta_0 - \eta}}, \qquad \text{(11.57 again)}$$

from which we can find the slip $\Delta w = -2w$ inside the crack in terms of the stress drop p inside the crack.

Let us assume, as before, that a semi-infinite crack suddenly appears for $x < 0$ at $t = 0$. Since, for $t < -x/\beta$ or $\eta < 0$, we expect no disturbance from the crack tip, the slip will be uniform under a uniform initial stress σ_{yz}^0. The slip for $\eta < 0$ can be expressed by equation (11.57) in terms of a uniform stress drop p_0, which is to be determined by the constitutive relation (11.63). Since the integration region is bounded by $t = 0$, $\xi_2(\eta) = -\eta$ for $\eta < 0$. Then equation (11.57) can easily be integrated to give

$$w(\xi_0, \eta_0) = \frac{-1}{\sqrt{2}\pi\mu} \int_{-\eta_0}^{\xi_0} \frac{d\xi}{\sqrt{\xi_0 - \xi}} \int_{-\xi}^{\eta_0} \frac{p_0\, d\eta}{\sqrt{\eta_0 - \eta}} = -\frac{\beta p_0 t}{\mu} \qquad \text{on } y = 0^-,$$

where (11.48) has been used. From equation (11.63), we have

$$\sigma_{yz} = \sigma_{yz}^0 - p_0 = \gamma\,\Delta\dot{w} = -2\gamma\dot{w} = 2\gamma\beta p_0/\mu \qquad \text{for } \beta t < -x. \qquad (11.64)$$

This equation determines the stress drop p_0 occurring for $\beta t < -x$ in terms of the initial stress and the material constants, i.e.,

$$p_0 = \frac{\sigma_{yz}^0}{1 + 2\gamma\beta/\mu}.$$

For $\beta t > -x$ or $\eta > 0$, we can determine the stress drop $p(\xi, \eta)$ in essentially the same way as the above by solving (11.57) and (11.63) simultaneously. We must, however, use numerical methods to solve the integral equation (11.57). Since the integration range is limited to S_3, shown in Figure 11.20, the discretized integral equation can be solved in steps, in each of which the unknowns are $p(\xi_n, \eta_n)$ and $\dot{w}(\xi_n, \eta_n)$ at one discretized point

(n, m). Since $p(\xi_n, \eta_n)$ and $\Delta\dot{w} = -2\dot{w}(\xi_n, \eta_n)$ must be related by equation (11.63), the two equations can determine both p and $\Delta\dot{w}$ at the point.

In solving (11.57), the crack-tip location $\xi_2(\eta)$ must be known. Recognizing that $\xi = [\beta t - x_2(t)]/\sqrt{2}$ and $\eta = [\beta t + x_2(t)]/\sqrt{2}$ on the crack-tip locus, we have

$$\frac{d\xi_2}{d\eta} = \frac{d\xi_2/dt}{d\eta/dt} = \frac{\beta - \dot{x}_2(t)}{\beta + \dot{x}_2(t)}.$$

Then the equation (11.56) for the motion of the crack tip can be rewritten as

$$\frac{d\xi_2}{d\eta} = \frac{(2\pi\mu G)^2}{\left\{\int_{x_2-\beta t}^{x_2} p[x, t - (x_2 - x)/\beta]\frac{dx}{\sqrt{x_2 - x}}\right\}^4}. \tag{11.65}$$

The above equation is valid only when

$$\int_{x_2-\beta t}^{x_2} p[x, t - (x_2 - x)/\beta]\frac{dx}{\sqrt{x_2 - x}} \geq \sqrt{2\mu\pi G}, \tag{11.66}$$

otherwise the crack tip does not move and $x_2(t) = 0$. In that case,

$$\frac{d\xi_2}{d\eta} = 1. \tag{11.67}$$

The condition (11.66) can be checked by a numerical integration of discretized $p(\xi_n, \eta_n)$. Then, either (11.65) or (11.67) is used to determine the locus of the crack tip by

$$\xi_2(\eta_{m+1}) = \xi_2(\eta_m) + \frac{d\xi_2}{d\eta}\Delta\eta,$$

where $\Delta\eta$ is the grid spacing in η.

Ida (1973) made numerical calculations for various choices of the parameters v_c, γ, and σ_{yz}^d, and found two distinctly different types of rupture propagation, depending on the parameter values. One type is a smooth rupture propagation in which, once the rupture starts, the crack tip accelerates smoothly and approaches the shear velocity. An example of smooth propagation is shown in Figure 11.23. Here the time t is measured in units of $t_c = \pi\mu G/2\beta p_0^2$. This is the delay time given in (11.59), which corresponds to the stress drop given in (11.64). We discussed the magnitude of t_c in earthquakes in the previous example of a semi-infinite crack that stops. The distance x is measured in units of βt_c, and the numbers in Figure 11.23 represent $\sigma_{yz}(x, t)$ in units of p_0. The parameters are chosen as $\gamma = 2\mu/\beta$, $v_c = 2.1 \times (\beta p_0/\mu)$, and $\sigma_{yz}^d = 0$. In the case of smooth rupture propagation, the cracked region (for which $\sigma_{yz} = 0$ in this case of $\sigma_{yz}^d = 0$) extends in both directions.

For a slightly different choice of parameters, the mode of rupture propagation can be quite different. The result is shown in Figure 11.24 for $\gamma = 2\mu/\beta$, $v_c = 2.6 \times (\beta p_0/\mu)$, and $\sigma_{yz}^d = 0$. The rupture propagation is quite irregular; the crack tip moves for a short distance, then stops, restarts, and repeats the process. The fault, once cracked, can be quickly healed,

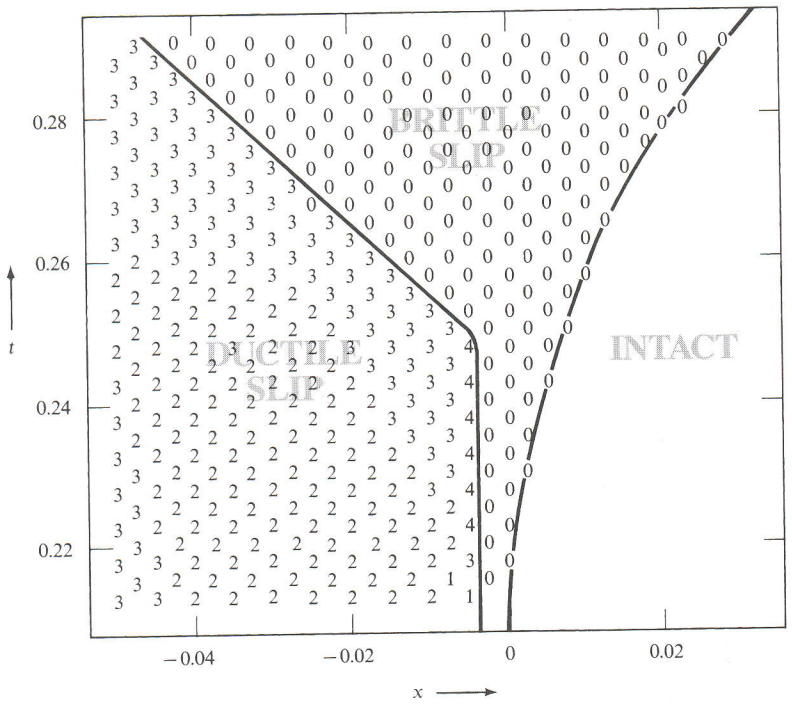

FIGURE **11.23**
Plot of $\sigma_{yz}(x,t)$ in units of p_0. A smooth propagation occurs in this case. [From Ida, 1973; copyright by the American Geophysical Union.]

because the slip rate drops below v_c. Thus the healing front follows the crack tip with a similar speed, making the effective crack length always roughly constant.

As discussed in Chapter 10, the high-frequency spectrum of seismic waves in the far field consists primarily of contributions from rupture nucleation and stopping points. We therefore anticipate a long duration of complex high-frequency waves from an irregular rupture process such as shown in Figure 11.24. On the other hand, a smooth earthquake like the one shown in Figure 11.23 will generate large long-period waves, with distinct short-period phases associated with the initial start and the final stopping points.

Ida's result indicates that the smooth type of rupture occurs when μ/β (the impedance associated with plane shear waves—see Box 5.4) is only a small multiple of p_0/v_c. Thus, roughly speaking, the smooth type of fault propagation occurs when the impedance in the creep region is higher than in the elastic region. For a given value of v_c, the smooth type of rupture occurs at lower frictional stress σ_{yz}^{d}.

Cohesionless crack

Burridge and Halliday (1971) considered an anti-plane crack that nucleates along a line at a constant depth in a homogeneous half-space. The crack propagates vertically both upward and downward. Their fracture criterion is a special case of (11.56), in which the

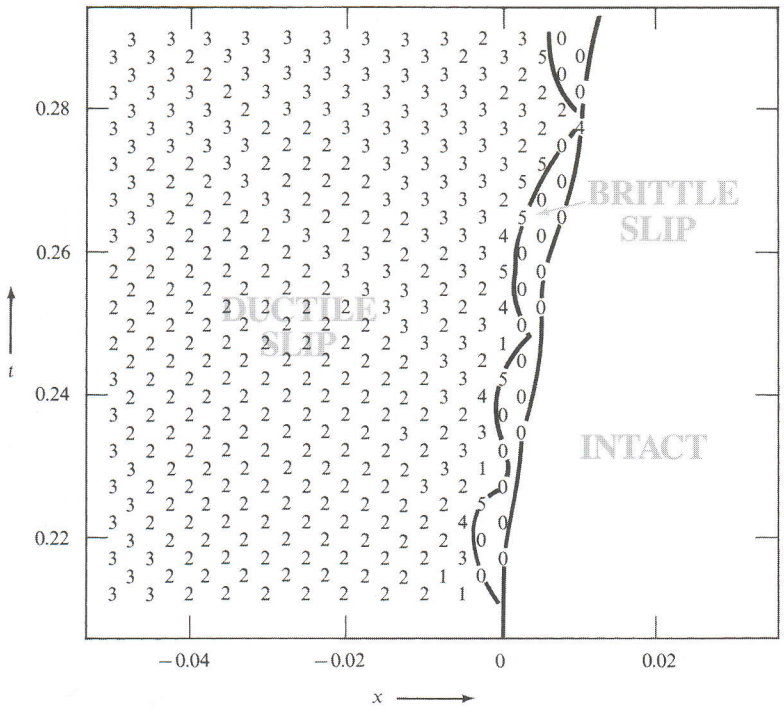

FIGURE **11.24**
Plot of $\sigma_{yz}(x,t)$ in units of p_0. A case of irregular propagation. [From Ida, 1973; copyright by the American Geophysical Union.]

specific surface energy G is set to zero. From (11.56), the condition that $G = 0$ can be met either by

$$v = \beta$$

or by

$$\int_{x_2-\beta t}^{x_2} p[x, t-(x_2-x)/\beta]\frac{dx}{\sqrt{x_2-x}} = 0. \tag{11.68}$$

Equation (11.68) is possible only if $p(x,t)$ changes sign along the above integration path. If (11.68) is not met, the crack tip must propagate with the shear velocity β. To slow down a propagating crack, therefore, one must postulate a negative stress drop. Taking the x-axis vertically downward, Burridge and Halliday considered the stress drop given by

$$p(x,t) = p_0(1 - x^2/b^2), \tag{11.69}$$

where p_0 is a constant. The crack tip propagates downward and past the depth b with the velocity β until the contribution from negative p matches that from positive p to satisfy equation (11.68). Then the crack tip moves deeper with a velocity determined by

equation (11.68). Thus the stress along the fault plane above the depth b drops to a lower value, but that below b jumps to a higher value. We shall come back to the cohesionless fracture in the discussion of in-plane cracks in the next section.

11.2.3 SPONTANEOUS PROPAGATION OF AN IN-PLANE SHEAR CRACK

Let us now consider spontaneous propagation of an in-plane shear crack. As in the anti-plane case, the crack lies on the plane $y = 0$, extending to infinity in the z-direction but confined in the x-direction between $x_1(t)$ and $x_2(t)$ at time t. For the in-plane case, the nonvanishing displacement components are $u(x, y, t)$ and $v(x, y, t)$ (see Section 10.2.4). As in the anti-plane case studied in Section 11.2.1, we assume that initially the crack is absent and that the body is in equilibrium with an initial state of stress $\boldsymbol{\sigma}^0$. We shall take this initial state as the reference state and measure the displacement relative to it. The initial conditions are then given by

$$u = v = 0 \qquad \text{and} \qquad \frac{\partial u}{\partial t} = \frac{\partial v}{\partial t} = 0 \qquad \text{for} \quad t < 0.$$

The total stress is then $\boldsymbol{\sigma} = \boldsymbol{\sigma}^0 + \boldsymbol{\tau}$. When the crack is formed, σ_{xy} on the crack drops from σ^0_{xy} to the dynamic frictional stress σ^{d}_{xy}. Putting the stress drop $\sigma^0_{xy} - \sigma^{\mathrm{d}}_{xy} = p(x, t)$, the boundary condition for incremental stress on the crack appropriate for the above choice of reference state is given by

$$\tau_{xy} = -p(x, t) \qquad x_t(t) < x < x_2(t),\ y = 0. \tag{11.70}$$

As shown in Section 10.2.4, the continuity of $v(x, y, t)$ and $\tau_{xy}(x, y, t)$ across $y = 0$ leads to symmetries such that $u(x, y, t)$ and $\tau_{yy}(x, y, t)$ are odd functions of y and $v(x, y, t)$ and $\tau_{xy}(x, y, t)$ are even functions of y. Since τ_{yy} is continuous across $y = 0$,

$$\tau_{yy} = 0 \qquad y = 0. \tag{11.71}$$

We need another condition on $y = 0$ outside the crack. This is given by the continuity of u. Since a continuous odd function of y must vanish at $y = 0$, we have

$$u = 0 \qquad x < x_1(t), x_2(t) < x,\ y = 0. \tag{11.72}$$

(11.70) and (11.72) taken together are a mixed boundary condition on $y = 0$, and (11.71) gives the other boundary condition for all x on $y = 0$. Because of the symmetry, it is sufficient to obtain a solution only in the half-space $y < 0$.

We shall define the two-dimensional Green functions $g_{x\xi}(x, y, t; \xi, y, \tau)$ and $g_{y\xi}(x, y, t; \xi, y, \tau)$, for a homogeneous half-space $y \leq 0$ with free surface at $y = 0$, as the displacement components u and v observed at (x, y, t) due to a line-impulsive force applied at (ξ, y, τ) in the ξ-direction. Then, from the representation theorem (2.43),

since our $g_{x\xi}, g_{y\xi}$ satisfy the stress-free boundary condition, and since $\tau_{yy} = 0$ on $y = 0$, we have

$$u(x, y, t) = \iint_S \tau_{xy}(\xi, \tau) g_{x\xi}(x, y, t; \xi, 0, \tau)\, d\xi\, d\tau,$$
$$v(x, y, t) = \iint_S \tau_{xy}(\xi, \tau) g_{y\xi}(x, y, t; \xi, 0, \tau)\, d\xi\, d\tau.$$

The region of integration S is, from causality, that region of the (ξ, τ) plane for which

$$\alpha^2(t - \tau)^2 - (x - \xi)^2 - y^2 \geq 0 \qquad t \geq \tau \geq 0,$$

where α is the P-wave velocity. The above representation is valid also for displacements on the crack plane $y = 0^-$, in which we are particularly interested. In this case, the region of integration is a triangle S_0 in the (ξ, τ) plane given by

$$\alpha^2(t - \tau)^2 - (x - \xi)^2 \geq 0 \qquad t \geq \tau \geq 0,$$

and we write

$$\begin{aligned} u(x, 0, t) &= \iint_{S_0} \tau_{xy}(\xi, \tau) g_{x\xi}(x - \xi, 0, t - \tau)\, d\xi\, d\tau, \\ v(x, 0, t) &= \iint_{S_0} \tau_{xy}(\xi, \tau) g_{y\xi}(x - \xi, 0, t - \tau)\, d\xi\, d\tau. \end{aligned} \tag{11.73}$$

This notation for the Green function refers to the case of a homogeneous half-space when source (ξ, η, τ) and receiver (x, y, t) are both on the free surface. Explicit formulas for $g_{x\xi}$ and $g_{y\xi}$ are easily derived by Cagniard's method (Section 6.4), and they are particularly simple when $y = \eta = 0$. The result for this case is

$$\begin{aligned} g_{x\xi}(x, 0, t) &= \frac{4\sigma^2}{\pi\mu\beta^2 x} \frac{(\sigma^2 - \beta^{-2})\sqrt{\sigma^2 - \alpha^{-2}}}{\mathsf{R}(\sigma)\mathsf{R}^*(\sigma)} && \frac{1}{\alpha} < \sigma < \frac{1}{\beta} \\ &= \frac{1}{\pi\mu\beta^2 x} \frac{\sqrt{\sigma^2 - \beta^{-2}}}{\mathsf{R}(\sigma)} && \frac{1}{\beta} < \sigma, \\ g_{y\xi}(x, 0, t) &= \frac{K_I}{\mu}\delta\left(t - \frac{x}{c_{\mathrm{R}}}\right) + \frac{2\sigma}{\pi\mu\beta^2 x} \frac{(2\sigma^2 - \beta^{-2})\sqrt{\sigma^2 - \alpha^{-2}}\sqrt{\beta^{-2} - \sigma^2}}{\mathsf{R}(\sigma)\mathsf{R}^*(\sigma)}, \end{aligned} \tag{11.74}$$

where $\sigma = t/x$, β is the velocity of shear waves, R is the Rayleigh function

$$\mathsf{R}(\sigma) = (2\sigma^2 - \beta^{-2})^2 - 4\sigma^2\sqrt{\sigma^2 - \alpha^{-2}}\sqrt{\sigma^2 - \beta^{-2}},$$

R^* and K_I are defined by

$$\mathsf{R}^*(\sigma) = (2\sigma^2 - \beta^{-2})^2 + 4\sigma^2\sqrt{\sigma^2 - \alpha^{-2}}\sqrt{\sigma^2 - \beta^{-2}},$$

$$K_I = \frac{(2\beta^2/c_{\mathrm{R}}^2 - 1)^3}{\dfrac{16\beta^2}{c_{\mathrm{R}}^2}\left[1 - \left(6 - 4\dfrac{\beta^2}{\alpha^2}\right)\dfrac{\beta^2}{c_{\mathrm{R}}^2} + 6\left(1 - \dfrac{\beta^2}{\alpha^2}\right)\dfrac{\beta^4}{c_{\mathrm{R}}^4}\right]},$$

and c_{R} is the velocity of Rayleigh waves ($\mathsf{R}(c_{\mathrm{R}}^{-1}) = 0$). Equation (11.74) was first derived by Lamb (1904).

If $\tau_{xy}(\xi, t)$ were known on the whole x-axis, equation (11.73) would give the solution of the problem. From the boundary condition (11.70), however, the stress component (11.72) is known only on the crack surface. Outside the crack, the boundary condition (11.72) is a constraint on the displacement component u. Separating the region of integration S_0 in (11.73) into a part S_1 inside the crack $[x_1(t) < x < x_2(t)]$, for which τ_{xy} is known by (11.70), and a part S_2, we can rewrite the condition (11.72) as

$$\iint_{S_1} p(\xi, \tau) g_{x\xi}(x - \xi, 0, t - \tau)\, d\xi\, d\tau \tag{11.75}$$

$$= \iint_{S_2} \tau_{xy}(\xi, \tau) g_{x\xi}(x - \xi, 0, t - \tau)\, d\xi\, d\tau \qquad \begin{array}{l}\text{for } x < x_1(t) \\ \text{or } x_2(t) < x.\end{array}$$

Kostrov (1975) obtained an analytic solution of the above equation. The result, however, is much more involved than in the case of an anti-plane crack. For example, the stress-intensity factor given by only one integration in the anti-plane case (equation (11.55)) now requires five integrations and one differentiation. Besides, the result is valid only for a crack-tip velocity less than the Rayleigh-wave velocity. It therefore appears that a numerical approach may be more satisfactory.

A sophisticated method of discretizing the integral equations (11.73) and (11.75) was described by Burridge (1969). However, a more conventional method, such as the one used by Hamano (1974), reproduces Burridge's result quite closely. In Hamano's method, the x-axis is divided into segments of equal interval d, and each segment is presumed to take the average value of stress and displacement over the segment. Then it is natural to replace the point-to-point Green function $g(x - \xi, 0, t - \tau)$ by a segment-to-segment Green function $\bar{\bar{g}}(x_i - \xi_j, 0, t - \tau)$, which is the averaged displacement over the ith segment due to the force distributed over the jth segment:

$$\bar{\bar{g}}(x_i - \xi_i, 0, t - \tau) = \frac{1}{d^2}\int_{x_i - (d/2)}^{x_i + (d/2)} dx \int_{\xi_j - (d/2)}^{\xi_j + (d/2)} g(x - \xi, 0, t - \tau)\, d\xi. \tag{11.76}$$

For $g_{x\xi}(x, 0, t)$ given in (11.74), $\bar{\bar{g}}_{x\xi}(x, 0, t)$ can be obtained in a compact form, as given in Das and Aki (1977a). Using the averaged Green function, the integral equation (11.75) can be discretized as

$$\sum_{\substack{j \\ \text{in}}} \sum_{\substack{l \\ S_1}} p(\xi_j, \tau_l)\bar{\bar{g}}_{x\xi}(x_i - \xi_j, t_k - \tau_l) = \sum_{\substack{j \\ \text{in}}} \sum_{\substack{l \\ S_2}} \tau_{xy}(\xi_j, \tau_l)\bar{\bar{g}}_{x\xi}(x_i - \xi_j, t_k - \tau_l) \quad \begin{matrix} \text{for } x_i < x_1(t_k) \\ \text{or } x_2(t_k) < x_i. \end{matrix} \tag{11.77}$$

The order of solving the above set of equations in Hamano's method can be arranged so that there is only one unknown, $\tau_{xy}(\xi_j, \tau_l)$, when each equation is solved. Once τ_{xy} is determined for the whole region, the displacement can be calculated by the discretized equation (11.73).

So far, we have been proceeding as if the locations of crack tips $x_1(t)$ and $x_2(t)$ were known. But these locations are determined by some fracture criterion. The simplest criterion that can be easily incorporated in the discretized formulation (11.77) is to monitor the stress difference between the neighboring grid points that bracket the position of the crack tip. The total stress at the point inside the crack is known to be σ_{xy}^{d}, and that outside is determined as $\sigma_{xy}^{0} + \tau_{xy}$ by solving (11.77) for the incremental stress τ_{xy}. Thus the excess of stress outside the crack over that inside is $\tau_{xy} + \sigma_{xy}^{0} - \sigma_{xy}^{\mathrm{d}} = \tau_{xy} + p$. As soon as this stress difference exceeds a certain limit S_{c}, i.e.,

$$\tau_{xy} - \sigma_{xy}^{\mathrm{d}} + \sigma_{xy}^{0} \geq S_{\mathrm{c}}, \tag{11.78}$$

we presume that rupture takes place. The crack tip advances beyond the point at which the stress difference had been exceeded, and the stress at the point is set to σ_{xy}^{d}. The stress difference across the crack tip may be considered as a smeared-out stress concentration. We know from equation (11.7) that the stress concentration takes the form

$$\sigma = \frac{K'}{\sqrt{2\pi x'}} H(x'),$$

where $x' = x - vt$ is the distance measured from the crack tip and K' is the stress-intensity factor for in-plane cracks. Suppose that the crack tip lies halfway between two grid points as shown in Figure 11.25. Then the average stress over the grid immediately outside the tip will be

$$\bar{\sigma} = \frac{1}{d}\int_0^d \frac{K'}{\sqrt{2\pi x'}}\, dx' = 2\frac{K'}{\sqrt{2\pi d}}.$$

In Box 11.2, we introduced Irwin's fracture criterion, which is based on the critical intensity factor K_{c}. The critical average stress $\bar{\sigma}$ over the grid immediately outside the tip corresponding to K_{c} may be written as

$$S_{\mathrm{c}} = 2\frac{K_{\mathrm{c}}}{\sqrt{2\pi d}}. \tag{11.79}$$

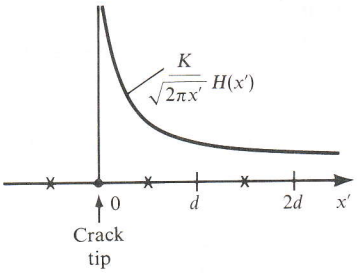

FIGURE **11.25**
Grid points are shown by X symbols.

Das and Aki (1977a) compared a numerical solution based on the criterion for S_c and an analytic solution based on the criterion for K_c for the case of a semi-infinite, anti-plane crack. Figure 11.21 shows the analytic solution as solid curves and the numerical solution as step-like curves. The symbol T_c attached to the analytic solution is the rupture starting time t_c defined in (11.59), normalized to α/d as $T_c = \alpha t_c/d$. For an anti-plane crack the critical stress intensity factor K_c may be obtained by setting $v = 0$ in (11.22), i.e., $K_c^2 = 4\mu G$. Then, from (11.59), we have $\beta t_c = (\pi/2)K_c^2/(2\sigma_{yz}^2)^2$. The parameter S, used to specify the numerical solution, is related to S_c by $1 + S = S_c/(\sigma_{yz}^0 - \sigma_{yz}^d)$. If our assumed relation (11.79) is correct, we should find the relation between T_c and S is $T_c = (\pi/4)^2(\alpha/\beta)(1 + S)^2 \sim 1.07\,(1 + S)^2$, where we take into account the assumption $\sigma_{yz}^d = 0$ made in deriving (11.59). Figure 11.21 shows that equation (11.79) gives a good approximation to the actual value for large S. For small S, the constant factor in (11.79) must be slightly larger than 2. For the range of S from 0.5 to 5, the appropriate value of the constant varies from 2.10 to 2.53. For a given S_c, S can be increased by making the grid length smaller.

Thus the fracture criterion for the critical stress difference S_c may be approximately the same as the fracture criterion for the critical intensity factor, which we called Irwin's criterion in Box 11.2. As discussed in the Box, the Irwin and Griffith criteria are equivalent as far as the initiation of crack extension is concerned. However, for a finite rupture velocity, the two criteria are different, and the fracture criterion by S_c is not exactly the same as the Griffith criterion, resulting in different crack-tip motions as shown in Figure 11.21.

Das (1980) extended Hamano's discretization method to determine the slip function for general three-dimensional motion—that is, for slip in two dimensions on a fault plane within a homogeneous whole space, radiating a mix of anti-plane and in-plane motions into three dimensions. In some respects the problem is simpler than the analysis of shear stress by (11.77), and the subsequent determination of fault slip, because for the three-dimensional problem the basic Green functions corresponding to (11.74) are simpler. These 3D Green functions, the solutions to Lamb's problem for a point source when both source and receiver lie in the surface of a homogeneous half-space, become zero once the Rayleigh waves have passed. This results in a great reduction of the memory needed to store the Green functions, unlike the two-dimensional problem with a line source where the disturbance never ceases. The two-dimensional problem is of course simpler in physical terms because of the reduced number of relationships between stress and strain.

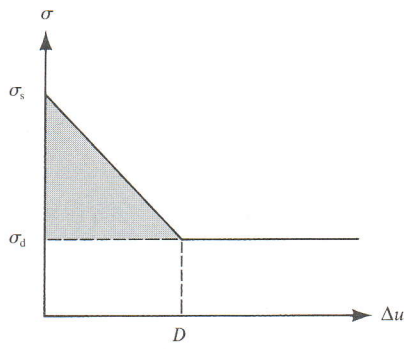

FIGURE **11.26**
Relation between shear stress and slip used by Ida (1972) and Andrews (1976). The static friction is σ_s: at this upper level of friction, instability begins and weakening occurs. For slip greater than D, stress drops to the dynamic friction level, σ_d. The shaded area corresponds to surface energy, i.e., the work done against the cohesive force (see Section 11.1.3). [After Andrews, 1976; copyright by the American Geophysical Union.]

Andrews (1976) used Ida's description of cohesive force to introduce the Griffith criterion (Section 11.1.3) into a finite-difference calculation of the in-plane shear-crack propagation. He assumed that traction across the fault plane is related to the slip Δu by the following formulas (see Figure 11.26):

$$\begin{aligned} \sigma(\Delta u) &= \sigma_s - (\sigma_s - \sigma_d)\,\Delta u/D \qquad && \Delta u < D, \\ \sigma(\Delta u) &= \sigma_d && \Delta u \geq D, \end{aligned} \tag{11.80}$$

where σ_s is the static friction, σ_d is the dynamic friction, and D is the slip required for stress to drop to σ_d. This is an example of what has come to be called a "slip-weakening" law. More specifically, it is a slip-weakening law with a constant weakening rate. The inelastic work done at the rupture front in excess of the work done against the dynamic frictional stress σ_d is identified as the specific surface energy (for each unit surface of newly created crack),

$$G = \tfrac{1}{4}(\sigma_s - \sigma_d)D. \tag{11.81}$$

The boundary condition on the fault plane must next be described. When the crack is not slipping,

$$\frac{\partial\,\Delta u}{\partial t} = 0 \qquad \text{and} \qquad |\sigma^0_{xy} + \tau_{xy}| \leq \sigma(\Delta u);$$

and during slip,

$$\frac{\partial\,\Delta u}{\partial t} \neq 0 \qquad \text{and} \qquad \sigma^0_{xy} + \tau_{xy} = \sigma(\Delta u)\ \text{sign}\left(\frac{\partial\,\Delta u}{\partial t}\right).$$

With this boundary condition, the propagation of a crack expands symmetrically in both the $+x$ and $-x$ directions. The results are discussed in terms of two nondimensional numbers: L_c/L and $(\sigma_s - \sigma_0)/(\sigma_0 - \sigma_d)$, where σ_0 is the initial stress σ^0_{xy} and L_c is the critical half-length of an in-plane Griffith crack, which can be obtained from equation (11.16).

Taking the limit as $v \to 0$, the critical stress intensity factor K_c will satisfy the following equation:

$$\begin{aligned} G &= \frac{g}{2v} \\ &= \frac{1}{16}\frac{K_c^2}{\mu\beta^2}\lim_{v\to 0}\frac{v^2}{\left(1-\frac{v^2}{\alpha^2}\right)^{1/2}-\left(1-\frac{v^2}{2\beta^2}\right)^2\left(1-\frac{v^2}{\beta^2}\right)^{-1/2}} \\ &= \frac{K_c^2}{8\mu}\frac{\lambda+2\mu}{\lambda+\mu}. \end{aligned} \tag{11.82}$$

From equation (9) of Box 11.1, the stress-intensity factor K' is related to the crack half-length L by $K' = (\sigma_0 - \sigma_d)\sqrt{\pi L}$. Therefore, the critical half-length L_c is given by

$$L_c = \frac{8\mu(\lambda+\mu)G}{\pi(\lambda+2\mu)(\sigma_0-\sigma_d)^2}. \tag{11.83}$$

Das and Aki (1977a) solved the same problem using Hamano's method, with the fracture criterion based on S_c, discussed earlier. In their case, L_c can be calculated by putting the value of K_c obtained from (11.79) into $K = (\sigma_0 - \sigma_d)\sqrt{\pi L}$ to find

$$L_c = d\frac{S_c^2}{2(\sigma_0-\sigma_d)^2}. \tag{11.84}$$

The other parameter, $(\sigma_s - \sigma_0)/(\sigma_0 - \sigma_d)$, is nothing but the parameter S used in the discussion of Figure 11.21:

$$S = \frac{S_c}{\sigma_0-\sigma_d} - 1 = \frac{\sigma_s-\sigma_d}{\sigma_0-\sigma_d} - 1 = \frac{\sigma_s-\sigma_0}{\sigma_0-\sigma_d}. \tag{11.85}$$

The results of calculation by the two methods agree in general, and only Andrew's result is reproduced in Figure 11.27. There are two distinct styles of rupture propagation. If the parameter S is greater than about 1.63, the velocity of rupture propagation is always less than the Rayleigh-wave velocity c_R, and the velocity approaches c_R as the crack length increases. On the other hand, if S is less than 1.63, the rupture starts with sub-Rayleigh velocity. But as the crack length exceeds a certain limit (which depends on S), the rupture velocity exceeds the shear velocity and approaches the P-wave velocity as the crack length increases. The critical value of $S = 1.63$ was obtained by Burridge (1973), using the cohesionless fracture criterion discussed in the example of anti-plane crack propagation (see the last part of Section 11.2.2). The cohesionless crack cannot propagate at velocities lower than the Rayleigh-wave velocity because of its inability to sustain any stress singularity. It can propagate with the Rayleigh velocity, at which speed the stress-intensity factor is zero. Burridge, however, showed that even at the Rayleigh velocity, the stress ahead of the crack at the S-wave front may exceed the static friction if S is less than 1.63. In that case, the admissible speed of the crack tip is the P-wave velocity. In Section 11.1.2, we concluded from the study of energetics at the crack tip that the speed of an in-plane crack cannot

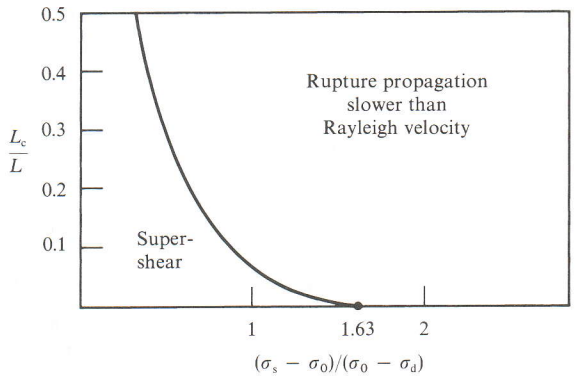

FIGURE **11.27**
Showing separate regions in which rupture propagates with sub-Rayleigh velocity, and with super-shear velocity. [After Andrews, 1976; copyright by the American Geophysical Union.]

exceed the Rayleigh-wave velocity. For a cohesionless crack, the stress-intensity factor is always zero and there is no energy flow through the crack tip. Therefore, the conclusion from the energetics does not apply to a cohesionless crack. A more difficult question is why the numerical solutions, which apparently involve a finite energy flow through the crack tip (as demonstrated by the agreement with analytic solutions for such cases), show rupture-propagation velocities exceeding that of Rayleigh waves. The answer lies in their fracture criterion, in which the initiation of fault slip does not require an infinite stress but only a finite stress, Thus, the stress associated with P- and S-waves propagating ahead of a crack tip can cause the fault slip. Hence we may say that the super-Rayleigh-wave velocity propagation is a consequence of finite cohesive forces.

The finite cohesive force has another important consequence on what happens when the rupture propagates along a fault plane with obstacles or barriers. These barriers may be expressed by a localized high value of S_c defined in (11.78). Das and Aki (1977b) found that three different situations can occur when a crack tip passes such a barrier, depending on the relative magnitude of barrier strength to initial stress:

(i) If the initial stress is relatively high, the barrier is broken immediately.

(ii) If the initial stress is relatively low, the crack tip proceeds beyond the barrier, leaving behind an unbroken barrier.

(iii) If the initial stress is intermediate, the barrier is not broken at the initial passage of the crack tip, but eventually breaks due to a later increase in stress.

If the barrier encounter of type (i) occurs throughout the fault plane, rupture propagation is smooth, generates a simple impulsive seismic signal, and results in a high average stress drop. On the other hand, if the type (ii) encounter occurs at many barriers, rupture propagation becomes rough, generates a long sequence of high-frequency waves, and ends up with a low average stress drop. Type (iii) propagation generates seismograms with ripples superimposed on long-period motion. The seismic radiation becomes less dependent on direction of rupture propagation than others, because the slip on the central part of the crack occurs more or less simultaneously, resulting in an effectively symmetric source. Similar results were obtained by Mikumo and Miyatake (1978), who studied rupture propagation over a fault plane with a two-dimensional nonuniform distribution of static friction.

Thus, a variety of rupture processes can be generated by distributing a number of barriers with different strengths on the fault plane to serve as more complex models of actual earthquakes. The fault model with barriers is particularly important for the study of short-period motions from a large earthquake, because it is associated with strong ground motion in the frequency band that is most damaging to man-made structures.

Our numerical methods of solving for fault slip in this chapter have included both finite difference methods as in Section 11.1.5, in which seismic motions are propagated throughout a volume, and so-called boundary integral methods such as those of the present Section 11.2.3, in which calculations of displacement and stress are confined only to the plane of the fault itself (via (11.73) and (11.75)). Bizzani *et al.* (2001) have thoroughly studied the slip distribution for two-dimensional in-plane shear rupture governed by the slip-weakening law shown in Figure 11.26, and also by more general rate- and state-dependent friction laws proposed by Dieterich and Ruina. They find the two numerical methods of solving for fault slip lead to identical solutions if care is taken to ensure numerical stability and adequate resolution. Their boundary integral method, developed by Andrews (1985), was faster than their finite difference method.

11.3 Rupture Propagation Associated with Changes in Normal Stress

Many times in the solutions discussed above we have made use of the fact that shear discontinuities on a planar fault surface, in a homogeneous isotropic elastic whole space, cannot change the normal stress on the fault. See Problem 10.2. (This constancy of normal stress does not mean that the original planar fault surface stays flat. In practice it warps during slip in a fashion that keeps the normal stress unchanged.) The constancy of normal stress simplifies the discussion of shearing stresses on the fault plane, since in practice we can relate shearing stress via a coefficient of friction to the normal stress. Because the normal stress cannot change, changes in the coefficient of friction are directly reflected as changes in the shear stress. But this simplification is lost if the fault surface is nonplanar, or if the fault surface is itself a material discontinuity between media with different elastic moduli, or if the fault is shallow. In the latter case, seismic motions will be reflected from the Earth's free surface, back down into the source region. If the reflections reach the fault while it is still in the process of slipping, then the normal stress on the fault will be changed in ways that can influence the process of slip. In this section, we briefly review each of these three possibilities for changing the normal stress.

If the fault surface is bumpy, then resistance to slip may be greater due to the possibilities of indentation of material on one side of the fault into the other. Conceptually such a fault can lock, and a new plane of weakness can develop nearby. Models of such an asperity can be developed in terms of a spatially varying coefficient of friction applied over a planar fault, so that greater shear stress is needed to accomplish slip near the location of the indentation. But such an approach does not reproduce the fact that normal stress across the fault will change as an asperity begins to slip. Bouchon and Streiff (1997) considered a generalized version of the spontaneous rupture model discussed above in Section 11.2. They allowed for nonplanar faulting by assuming that shear stress at the time of nucleation drops from its initial static level to the value given by a dynamic coefficient of friction times the original normal stress. For a fault with a bend, their boundary integral method allows for friction

that varies as the dynamic normal stress changes continuously. But Tada and Yamashita (1996) have pointed out fundamental differences in behavior for in-plane shear cracks that are nonplanar, between cracks that change their orientation smoothly from point to point, and cracks with an abrupt kink (discontinuous change in fault normal). They found that the normal stress along a smoothly curved crack differs from that along a chain of line segments connected at abrupt kinks (the chain being a discrete version of the smooth variation).

Faults that have endured numerous earthquakes over millions of years can accumulate many kilometers of offset, bringing rocks of quite different composition—and different elastic properties—into contact. When a new episode of slip occurs across a surface that is also a material discontinuity, the resulting wavefields are significantly more complicated than the usual P and S body waves. For example, head waves can propagate along the faster side of the interface, delivering energy into the slower (more compliant) medium by refraction at a critical angle. This energy arrives earlier and from a different direction than would be the case if slip occurred only within a homogeneous block of the slower medium. Ben-Zion and Malin (1991) showed for the San Andreas fault, in central California, that such head waves have sometimes been misinterpreted as body waves arriving directly from an earthquake hypocenter, leading to erroneous estimates of the hypocenter location. Weertman (1980) showed that for a dislocation moving along a material interface at constant speed, the change in normal stress increases with increasing dislocation velocity up to the speed of the S-wave in the slower medium. Andrews and Ben-Zion (1997) used a finite difference method for two-dimensional plane strain to study slip between materials that had a 20% contrast in elastic wave speeds, and found features similar to those predicted by Weertman. They showed that a self-sustaining and spatially narrow pulse of slip, associated with a tensile change of normal stress, could propagate at about the velocity of the slower S-wave speed. The direction of propagation is always the same as the direction of slip in the slower medium.

The phenomenon of tensile changes in normal stress has also been found for slip on planar faults in homogenous media. These tensile changes, which can be large enough to cause separation of the two surfaces of the fault, arise in laboratory experiments conducted by Brune and coworkers. They used foam rubber blocks in a geometry that simulated shallow-angle thrust faulting. Mora and Place (1994) modeled the geometry of the foam block experiments using a numerical lattice model, and also found interface waves associated with tensile changes in normal stress that tended to separate the fault surfaces. The reason for such changes in normal stress is presumably the interaction between fault motions on the shallow fault and motions reflected from the free surface, which cause tensile changes on the fault plane. Brune *et al.* (1993) found that the observed particle motions show several features very different from those commonly found for planar dislocations within a whole space. Interface waves associated with fault opening propagate updip along the thrusting fault plane, and temporarily decouple the hanging wall from the foot wall. Seismic energy becomes trapped in the overlying wedge, and consequently the particle motions are asymmetrical, being far greater in the hanging wall than the foot wall. The energy becomes increasingly concentrated toward the tip of the upper wedge—the toe of the hanging wall—leading to what these experimenters call spectacular breakout phases when the rupture reaches the free surface. Their results suggest that the seismic hazard of great subduction zone thrust earthquakes, and continental shallow angle thrust faults, may

be significantly greater than would be predicted by standard dislocation models that do not take into account the interactions of fault rupture with a nearby free surface.

Throughout our chapters on source theory, we have focused on models that apply to individual earthquakes. For each such model we have sought to explain how its associated fault slip and radiated motions can be analyzed. We have avoided the obvious fact that earthquakes occur in the setting provided by previous earthquakes. But each earthquake changes the stress environment in which it was triggered, dropping the stress over length scales comparable to the width and length of the fault-ruptured area. Each new earthquake, whether large or small, occurs in the inhomogeneous initial stress established by all its predecessors, though typically increased by tectonic loading. It is therefore of interest to determine how the balance is maintained between large earthquakes, which presumably tend to reduce stresses over wide regions, and small earthquakes, which introduce short wavelength inhomogeneities into the stress field. These underlying characteristics of the environment in which individual earthquake occur will determine the size of each new earthquake in a sequence. The overall relationship between earthquakes of different sizes may be governed by the principles of self-organized criticality. Earthquakes show properties that we still do not understand. It is a challenge to bring the wide range of observed earthquake phenomena into a complete and satisfactory framework established on basic physical principles.

Suggestions for Further Reading

Achenbach, J. D. On dynamic effects in brittle fracture. In *Mechanics Today*, vol. 1, edited by S. Nemat-Nasser, New York: Pergamon Press, 1974.

Andrews, D. J. Dynamic plane-strain shear rupture with a slip-weakening friction law calculated by a boundary integral method. *Bulletin of the Seismological Society of America*, **75**, 1–21, 1985.

Ben-Zion, Y., and D. J. Andrews. Properties and implications of dynamic rupture along a material interface. *Bulletin of the Seismological Society of America*, **88**, 1085–1094, 1998.

Bizzarri, A., M. Cocco, D. J. Andrews, and E. Boschi. Solving the dynamic rupture problem with different numerical approaches and constitutive laws. *Geophysical Journal International*, **144**, 656–678, 2001.

Bouchon, M., and D. Streiff. Propagation of a shear crack on a non-planar fault: A method of calculation. *Bulletin of the Seismological Society of America*, **87**, 61–66, 1997.

Cochard, A., and R. Madariaga. Dynamic faulting under rate-dependent friction. *Pure and Applied Geophysics*, **142**, 419–445, 1994.

Das, S., J. Boatwright, and C. H. Scholz, eds. *Earthquake Source Mechanics*. Geophysical Monograph 37, Maurice Ewing Series, vol. 6. Washington, D.C.: American Geophysical Union, 1986.

Dieterich, J. H. A model for the nucleation of earthquake slip. In *Earthquake Source Mechanics*, edited by S. Das, J. Boatwright, and C. H. Scholz. Geophysical Monograph 37, Maurice Ewing Series, vol. 6, 37–47. Washington, D.C.: American Geophysical Union, 1986.

Ellsworth, W. L., and G. C. Beroza. Seismic evidence for an earthquake nucleation phase. *Science*, **268**, 851–855, 1995.

Freund, L. B. Crack propagation in an elastic solid subject to general loading. II. Non-uniform rate of extension. *Journal of Mechanics and Physics of Solids*, **20**, 141–152, 1972.

Freund, L. B. The mechanics of dynamic shear crack propagation. *Journal of Geophysical Research*, **84**, 2199–2209, 1979.

Geubelle, P., and J. R. Rice. A spectral method for 3D elastodynamic fracture problems. *Journal of Mechanics and Physics of Solids*, **43**, 1791–1824, 1995.

Liebowitz, H., ed. *A Treatise on Fracture,* vol. 2. New York: Academic Press, 1968.

Kostrov, B. V., and S. Das. *Principles of Earthquake Source Mechanics*. Cambridge University Press, 1988.

Madariaga, R. High frequency radiation from crack (stress drop) models of earthquake faulting. *Geophysical Journal of the Royal Astronomical Society*, **51**, 625–651, 1977.

Marone, C. Laboratory-derived friction laws and their applications to seismic faulting, *Annual Reviews of Earth and Planetary Sciences*, **26**, 634–696, 1998.

Orowan, E. Mechanism of seismic faulting. In *Rock Deformation*, edited by D. Griggs and J. Handin, Ch. 12. Geological Society of America, 1960.

Rice, J. R. A path independent integral and the approximate analysis of strain concentration by cracks and notches. *Journal of Applied Mechanics*, **35**, 379–386, 1968.

Rice, J. R., Y. Ben-Zion, and K. S. Kim. Three-dimensional perturbation solution for a dynamic planar crack moving unsteadily in a model elastic solid. *Journal of Mechanics and Physics of Solids*, **42**, 813–843, 1994.

Scholz, C. H. Earthquakes and friction laws. *Nature*, **391**, 37–42, 1998.

Zheng, G., and J. R. Rice. Conditions under which velocity-weakening friction allows a self-healing versus crack-like mode of rupture. *Bulletin of the Seismological Society of America*, **88**, 1466–1483, 1998.

Problems

11.1 If slip across a fault surface Σ is known as a function of position and time, is this enough to determine completely the motions throughout the medium within which the fault is situated (assuming no other source is active)? If your answer is "yes," then explain why this result is only of limited use in earthquake source theory. If your answer is "no," then describe what else must be known about the source in order to determine the motions that it radiates.

Suppose that, instead of the slip, we know the *traction* at all times on the part of the fault surface that is undergoing slip (i.e., on $\Sigma(t)$). Is this enough to determine the motion radiated away from the fault? Comment on your answer here (yes or no) in the same fashion requested above.

11.2 For the self-similar elliptical crack described in Sections 10.1.6 and 11.1.4, show that

a) the fault area grows like t^2,

b) the average slip grows like t,

c) the seismic moment grows like t^3, and hence that

d) the far-field velocity seismogram is proportional to $(t - t_P)H(t - t_P)$ near the arrival time $t = t_P$.

11.3 For a semi-infinite crack described as an example in Section 11.2.2, the stress-intensity factor K is given by

$$K = \frac{(1 - \dot{x}_2/\beta)^{1/2}}{\sqrt{\pi/2}} \int_{x_2 - \beta t}^{x_2} p(x, t - (x_2 - x)/\beta) \frac{dx}{\sqrt{x_2 - x}}$$

$$= \frac{2(1 - \dot{x}_2/\beta)^{1/2} \tau_0}{\sqrt{\pi/2}} \sqrt{\beta t}.$$

In that example, we derived the crack-tip motion assuming that the surface energy G is independent of rupture velocity. Show that if instead the critical stress intensity factor is constant (i.e., instead of G), then the crack-tip motion is given by

$$x_2(t) = \beta(t - t_c) - \beta t_c \log t/t_c.$$

This curve is shown in Figure 11.21 together with the curves corresponding to constant G.

11.4 For an in-plane tensile crack, the rupture propagation always has velocities lower than the Rayleigh velocity, even in the case of finite cohesive force. Confirm this conclusion by investigating the sense of stress associated with the P- and S-wave part of the Green function appropriate for a tensile crack.